Crystal structure classification of copper-based sulphides as a tool for the design of inorganic functional materials

P. Lemoine, Gabin Guelou, Bernard Raveau, Emmanuel Guilmeau

▶ **To cite this version:**

P. Lemoine, Gabin Guelou, Bernard Raveau, Emmanuel Guilmeau. Crystal structure classification of copper-based sulphides as a tool for the design of inorganic functional materials. Angewandte Chemie International Edition, 2022, 61 (2), pp.e202108686. 10.1002/anie.202108686 . hal-03333864v2

HAL Id: hal-03333864
https://hal.science/hal-03333864v2

Submitted on 9 Sep 2021

HAL is a multi-disciplinary open access archive for the deposit and dissemination of scientific research documents, whether they are published or not. The documents may come from teaching and research institutions in France or abroad, or from public or private research centers.

L'archive ouverte pluridisciplinaire **HAL**, est destinée au dépôt et à la diffusion de documents scientifiques de niveau recherche, publiés ou non, émanant des établissements d'enseignement et de recherche français ou étrangers, des laboratoires publics ou privés.

10.1002/anie.202108686

Crystal structure classification of copper-based sulphides as a tool for the design of inorganic functional materials

Pierric Lemoine,[+*[a]] Gabin Guélou,[+[b]] Bernard Raveau,[[b]] Emmanuel Guilmeau*[[b]]

[+] These authors contributed equally to this work
* Corresponding authors

[a] Dr P. Lemoine
ISCR, Univ. Rennes, CNRS, F-35000 Rennes, France
E-mail: pierric.lemoine@univ-rennes1.fr
[b] Dr G. Guélou, Prof B. Raveau, Dr E. Guilmeau
CRISMAT, ENSICAEN, UNICAEN, Normandie Univ, CNRS, 14000 Caen, France
E-mail: emmanuel.guilmeau@ensicaen.fr

Accepted Manuscript

Abstract

Research focusing on the interplay between structural features and transport properties in inorganic materials is of paramount importance for the identification, comprehension and optimisation of functional materials. In this respect, Earth-abundant copper sulphides have been receiving considerable attention from scientists as the urgency remains to discover and improve the efficiency of sustainable materials for energy applications. This proposed classification of copper sulphides, associated with block *p* and/or *d* elements, is based on their crystallographic features and the analysis of their transport properties. It provides guidelines to help estimating some properties of new materials (type of main charge carriers, thermal conductivity, transport mechanisms, etc.) by considering only their chemical composition and crystal structure. The classification relies essentially on recent work in the fields of thermoelectricity and photovoltaics and thorough crystal structure investigations.

1. Introduction

Over the past couple of decades, the generation of renewable and sustainable green energy has been at the centre of scientific attention because of the dramatic ramifications associated with greenhouse gas emissions and climate change.[1] It is undeniable that our current reliance on fossil energies has pushed us toward the edge of what ecosystems can withstand before collapsing altogether. It is in everyone's best interest to focus a large proportion of the scientific attention on finding more sustainable, renewable and cost-efficient green energy sources. In this regard, energies harvested from sunlight, wind, water streams, earth's crust or biomass will play an increasingly large role in the coming years. Another promising candidate with strong potential as a sustainable energy source is emerging with the recent developments in thermoelectric (TE) power generation.[2,3] This technology, unlike the aforementioned well-known energy sources, is still in the development stages with more progresses yet to be made. Nonetheless, thermoelectric devices already offer exceptional advantages such as reliability, simplicity and long-life expectancy. However, current state-of-the-art TE materials remain too expensive and/or inefficient for large scale production and devices are still limited to niche applications such as space exploration.[3,4]

Materials with high TE performances usually exhibit transport properties behaviour close to those of heavily doped semiconductors or semi-metals (charge carrier concentration between 10^{19} and 10^{21} cm^{-3}) alongside a low thermal conductivity. Additionally, large scale industrialisation and mass adoption of TE devices requires an easy manufacturing process of materials composed of cheap, non-toxic and widely available elements. Most ternary and quaternary copper sulphides, derivatives of natural minerals, exhibit such characteristics alongside typically complex structures that encourage low intrinsic thermal conductivities. Most of them can be easily doped to optimise the carrier concentration or are "intrinsic" degenerate semiconductors [3,5–11] Concomitantly, copper sulphides have shown interesting prospects for many other energy conversion and storage applications, such as thin film solar cells, dye synthesised solar cells, photocatalysis, batteries…[12–17]

Accepted Manuscript

The recent advances in copper sulphide thermoelectrics and photovoltaics have been achieved through a detailed analysis of the structure-property relationships. The rich chemistry originating from these crystal structures is crucial to the development of competitive energy harvesting technologies and thus, they must be well understood and described. In this regard, we propose to classify inorganic copper sulphides based on their respective structural characteristics and transport properties. This process will attempt to merge the current knowledge and extract important information about the nature of the chemical bond from the observed patterns. Ultimately, this original classification can be used as a powerful tool for the identification and investigation of promising materials for sustainable energy generation.

2. Crystal structure classification of inorganic copper sulphides

The discussed copper sulphide phases can be classified into five groups depending on the nature and coordination of the metal sulphide polyhedra and the complexity of their 3D ordering. In this review, the *M* atoms refer to the transition metals or metalloids that form the sphalerite-type (or wurtzite-type) network while *T* atoms always refer to the "interstitial" cations. While Cu atoms are systematically found in the sphalerite or wurtzite-type networks they are sometimes treated independently from *M* atoms for clarity.

The first four groups (A to D) include compounds for which the metal elements are in tetrahedral coordination with respect to sulphur following different long-range ordering characterized by either sphalerite ("abca" stacking of corner-sharing MS$_4$ tetrahedra layers) or wurtzite-type ("abab" stacking of corner-sharing MS$_4$ tetrahedra layers) network (Fig. 1). For compounds belonging to group A, the structures are characterized by a "simple" sphalerite or wurtzite-type network (Fig. 2a), whereas compounds in group B to D are characterised by *T* cations in "interstitial" positions of these sphalerite or wurtzite-type network (*i.e.* occupying some of the tetrahedral vacancies), giving rise to tetrahedral-octahedral [TS$_4$]M_6 complexes (Fig. 2b). These "interstitial" positions are unoccupied in structures of group A (Fig. 2a), partially occupied in structures of groups B (Fig. 2c) and C (Fig. 2d), and fully occupied in structures of group D (Fig. 2e). This leads to corner-sharing MS$_4$ tetrahedra network containing (i) isolated [TS$_4$]M_6 complexes in structures of group B (Fig. 2c), (ii) 1D, 2D, or 3D connected [TS$_4$]M_6 complexes in structures of group C (Fig. 2d), and (iii) an interpenetrated corner-sharing TS$_4$ tetrahedra network in structures of group D (Fig. 2e). Finally, the fifth group (group E) includes compounds composed of several types of polyhedra. The list of minerals and synthetic materials described in this work does not pretend to be exhaustive, instead only crystal structures that have been rigorously examined have been considered. This is particularly the case for group E compounds.

Accepted Manuscript

10.1002/anie.202108686

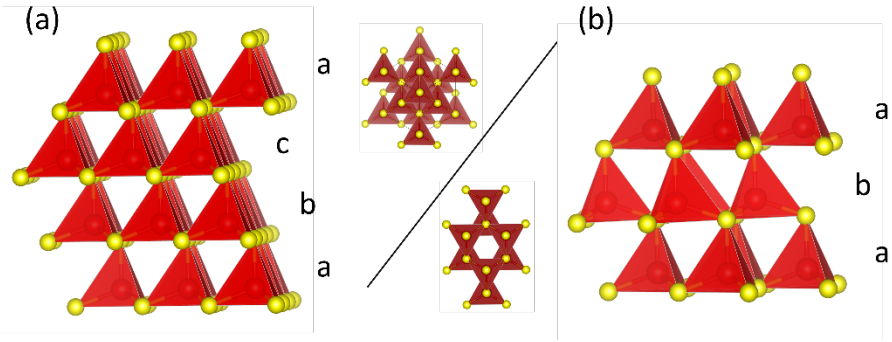

Figure 1 Schematic representations of the arrangement of MS$_4$ tetrahedra (red) in (a) sphalerite-type and (b) wurtzite-type structures.

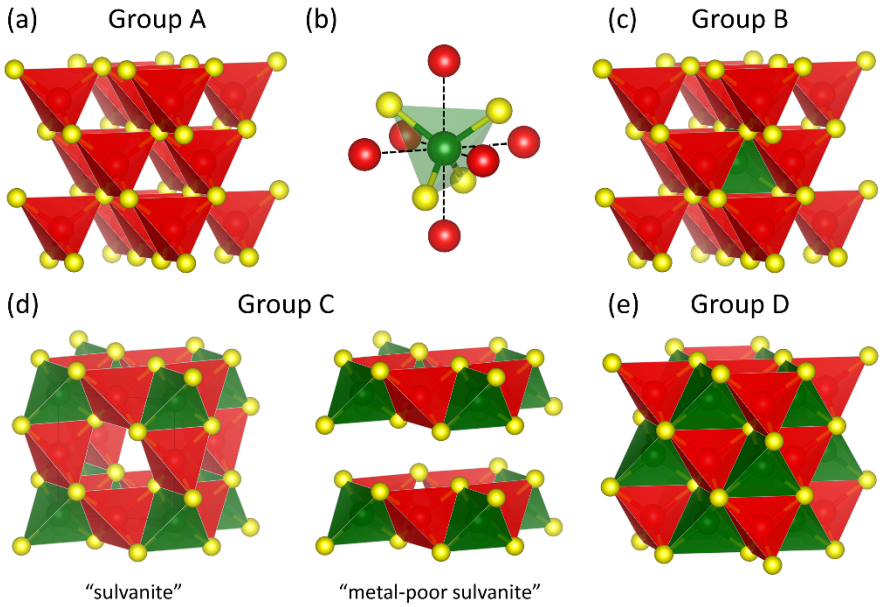

Figure 2 Schematic representations of the arrangement of (a) the group A sphalerite-type structures characterised by corner-sharing MS$_4$ (red) tetrahedra network; (b) the tetrahedral-octahedral [TS$_4$]M_6 complex with the "interstitial" T atom (green) forming TS$_4$ (yellow) tetrahedra associated with TM$_6$ (red) octahedra; (c) the group B sphalerite-type structures containing isolated [TS$_4$]M_6 complexes; (d) the group C sulvanite-type structures and metal-poor sulvanite-type derivatives containing [TS$_4$]M_6 complexes 3D and 2D connected, respectively; (e) the group D antifluorite-type structures characterised by two interpenetrating corner-sharing MS$_4$ (red) and TS$_4$ (green) tetrahedra networks, leading to a global corner- and edge-sharing (M,T)S$_4$ tetrahedra network.

The group A includes mineral phases or synthetic compounds characterised by a 3D arrangement of metal atoms in tetrahedral coordination of sulphur forming a non-centrosymmetric structure of corner-sharing tetrahedra. These structures are either derivatives of the sphalerite-type (also called zinc blende) structure ($F\bar{4}3m$, $a \approx 5.44$ Å and V ≈ 161 Å^3, Fig. 1a) or the wurtzite-type structure ($P6_3mc$, $a \approx 3.82$ Å, $c \approx 6.26$ Å and V ≈ 79 Å^3, Fig. 1b). There are many examples of compounds derived from sphalerite including phases with

Accepted Manuscript

disordered or semi-ordered cationic sublattices such as isocubanite $CuFe_2S_3$, kuramite Cu_3SnS_4 and kesterite Cu_2ZnSnS_4, but also ordered cationic sublattices such as chalcopyrite $CuFeS_2$, briartite Cu_2FeGeS_4, $CuGaS_2$, famatinite Cu_3SbS_4, stannite Cu_2FeSnS_4, roquesite $CuInS_2$, Cu_2GeS_3, mohite Cu_2SnS_3 and $Cu_5Sn_2S_7$, Table 1. An example of crystal structure with an ordered cationic arrangement is shown in Fig. 3a and b with the synthetic phase Cu_2GeS_3. Fewer examples can be found crystallising in the wurtzite-type structure such as synthetic phase Cu_3PS_4 and mineral enargite Cu_3AsS_4, Table 1.

Table 1 Structural information on group A phases.

Mineral	Composition	Space group	Cell parameters (Å)	Volume (Å^3)	$\overline{d_{M-S}}$ (Å)	Ref.
isocubanite	$CuFe_2S_3$	$F\bar{4}3m$	a = 5.295	148.5	2.293 ($Cu^+/Fe^{2+/3+}$)	[18]
kuramite	Cu_3SnS_4	$I\bar{4}2m$	a = 5.422 c = 10.826	318.3	2.334 (Cu/Sn)* 2.374 (Cu/Sn)* 2.345 (Cu)*	[19]
kesterite	Cu_2ZnSnS_4	$I\bar{4}2m$	a = 5.434 c = 10.856	320.6	2.332 (Cu^+) 2.334 (Cu^+/Zn^{2+}) 2.409 (Sn^{4+})	[20]
chalcopyrite	$CuFeS_2$	$I\bar{4}2d$	a = 5.289 c = 10.423	291.6	2.302 (Cu^+) 2.257 (Fe^{3+})	[21]
briartite	Cu_2FeGeS_4	$I\bar{4}2m$	a = 5.325 c = 10.51	298.0	2.300 (Cu^+) 2.349 (Fe^{2+}) 2.238 (Ge^{4+})	[22]
	$CuGaS_2$	$I\bar{4}2d$	a = 5.347 c = 10.474	299.5	2.312 (Cu^+) 2.288 (Ga^{3+})	[23]
famatinite	Cu_3SbS_4	$I\bar{4}2m$	a = 5.385 c = 10.754	311.9	2.316 (Cu^+) 2.406 (Sb^{5+})	[24]
stannite	Cu_2FeSnS_4	$I\bar{4}2m$	a = 5.450 c = 10.726	318.5	2.318 (Cu^+) 2.341 (Fe^{2+}) 2.414 (Sn^{4+})	[20]
roquesite	$CuInS_2$	$I\bar{4}2d$	a = 5.523 c = 11.133	339.6	2.334 (Cu^+) 2.465 (In^{3+})	[23]
	Cu_2GeS_3	Cc	a = 6.449 b = 11.319 c = 6.428 β = 108.37°	445.3	2.316 (Cu^+) 2.254 (Ge^{4+})	[25]
mohite	Cu_2SnS_3	Cc	a = 6.653 b = 11.537 c = 6.665 β = 109.39°	482.6	2.333 (Cu^+) 2.411 (Sn^{4+})	[26]
	$Cu_5Sn_2S_7$	$C2$	a = 12.058 b = 5.406 c = 8.503 β = 98.16°	548.7	2.299 ($Cu^{+/2+}$) 2.432 (Sn^{4+})§	[27]
	Cu_3PS_4	$Pmn2_1$	a = 7.282 b = 6.339 c = 6.075	280.4	2.324 (Cu^+) 2.070 (P^{5+})	[28]
enargite	Cu_3AsS_4	$Pmn2_1$	a = 7.43 b = 6.46 c = 6.18	296.6	2.321 (Cu^+) 2.218 (As^{5+})	[29]

* The refined chemical composition is reported with an under-stoichiometry on the anionic sublattice (*i.e.* $Cu_3SnS_{3.6}$) avoiding the estimation of the oxidation state of Cu and Sn atoms.

§ The existence of Sn_2S_7 dimers (SnS_4 tetrahedra linked two by two) in $Cu_5Sn_2S_7$ leads to one abnormally long Sn-S interatomic distance of 2.489 Å, and consequently, to a longer average Sn-S distance ($\overline{d_{Sn-S}}$) than that observed in other Sn^{4+}-containing phases of group A.

Accepted Manuscript

10.1002/anie.202108686

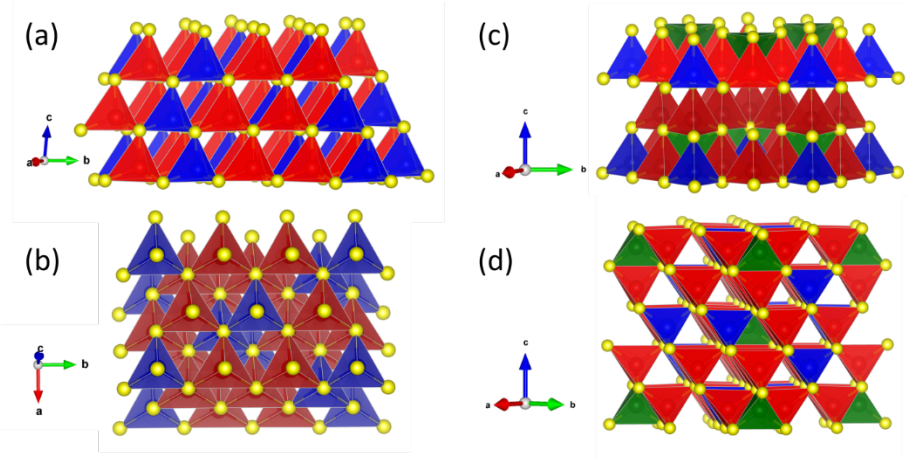

Figure 3 Schematic representations of the crystal structures of (a, b) group A Cu_2GeS_3 (Cc) and group B (c) catamarcaite Cu_6WGeS_8 ($P6_3mc$) and (d) colusite $Cu_{26}T_2M_6S_{32}$ ($P\bar{4}3n$, with T = Ti, V, Nb, Ta, Cr, Mo, W and M = Ge, Sn, As, Sb) with CuS_4 and MS_4 tetrahedra from the "host" structure in red and blue respectively, and the "intercalated" T cation at the centre of the TS_4 tetrahedra in green.

All the phases of group A are characterised by a M_{tot}/S ratio of 1 and a cationic sublattice composed of univalent Cu atoms, i.e. Cu(I) oxidation state (the presence of divalent copper Cu(II) is expected in kuramite Cu_3SnS_4 and in $Cu_5Sn_2S_7$), associated with another block *d* transition metal, a block *p* element, or a combination of both. Note that in these phases, the block *p* element is always in its d^{10} configuration. By considering the average interatomic distances $\overline{d_{M-S}}$ of the phases (Table 1) characterised by an ordered cationic sublattice *vs* the effective ionic Shannon radius of the cations in tetrahedral coordination (*i.e.* $r_{P^{5+}}$ = 0.17 Å, $r_{As^{5+}}$ = 0.335 Å, $r_{Ge^{4+}}$ = 0.390 Å, $r_{Ga^{3+}}$ = 0.47 Å, $r_{Fe^{3+}}$ = 0.49 Å, $r_{Sn^{4+}}$ = 0.55 Å, $r_{Sb^{5+}}$ = 0.565 Å, $r_{Cu^{+}}$ = 0.60 Å, $r_{In^{3+}}$ = 0.62 Å, and $r_{Fe^{2+}}$ = 0.63 Å)[30,31] we can observe two tendencies depending of the nature of the *M* element, *i.e.* either block *d* transition metal or block *p* element (Fig. 4). This indicates that (i) the aforementioned effective ionic radii of cations in tetrahedral coordination are well adapted for this class of materials and (ii) the nature of the chemical bonding between sulphur and block *d* transition metal, on one hand, and sulphur and block *p* element, on the other hand, is not strictly the same.

Accepted Manuscript

10.1002/anie.202108686

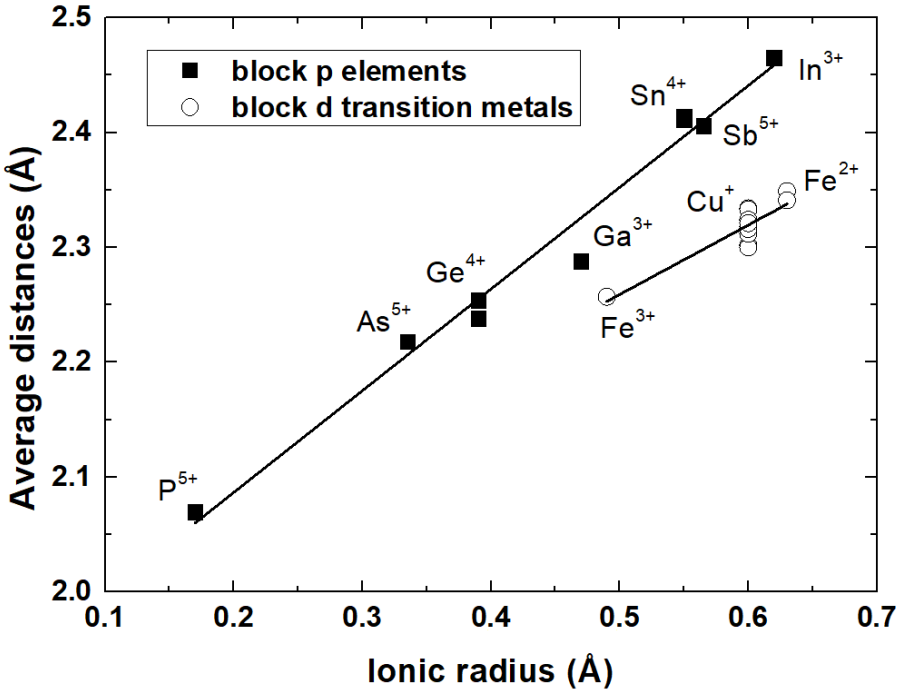

Figure 4 Average interatomic distances $\overline{d_{M-S}}$ of the group A phases characterised by an ordered cationic sublattice *vs* the effective ionic Shannon radius of the cations in tetrahedral coordination (*i.e.* $r_{P^{5+}}$ = 0.17 Å, $r_{As^{5+}}$ = 0.335 Å, $r_{Ge^{4+}}$ = 0.390 Å, $r_{Ga^{3+}}$ = 0.47 Å, $r_{Fe^{3+}}$ = 0.49 Å, $r_{Sn^{4+}}$ = 0.55 Å, $r_{Sb^{5+}}$ = 0.565 Å, $r_{Cu^{+}}$ = 0.60 Å, $r_{In^{3+}}$ = 0.62 Å, and $r_{Fe^{2+}}$ = 0.63 Å).[30,31] Due to its specific structural features, *i.e.* Sn_2S_7 dimers, the synthetic phase $Cu_5Sn_2S_7$ is not taken into account in this analysis.

Compounds from **group B** are similar to group A, thus exhibiting a sphalerite-type or wurtzite-type structure, with the additional occupancy of some interstitial tetrahedral sites by metal atoms. These atoms, "interstitial" with respect to the host structure, locally yield a structural feature derivative of the sulvanite structure ($P\bar{4}3m$, $a \approx 5.37$ Å, V ≈ 155 Å^3 [32]) where the interstitial cation is at the centre of a tetrahedral-octahedral [TS$_4$]M_6 complex (Fig. 2b). The resulting tetrahedra thus share their edges with the tetrahedra from the host structure (Fig. 2c). This particular crystal chemistry feature generates short distances between the interstitial cation T and the surrounding 6 M cations from the host structure. This suggests that particular unconventional donor-acceptor T-M bonds are formed in the tetrahedral-octahedral [TS$_4$]M_6 complexes due to direct overlapping of the d orbitals between the central d^0 T cation and the d^n M (Cu^+, Fe^{3+}/Fe^{2+}) cations. In group B, these tetrahedral-octahedral complexes are isolated from one another (Fig. 5a) forming a 0D array of complexes in a sphalerite/wurtzite-type network. This group B thus includes compounds crystallising in non-centrosymmetric complex structure including isolated tetrahedral-octahedral [TS$_4$]M_6 complexes.

Accepted Manuscript

10.1002/anie.202108686

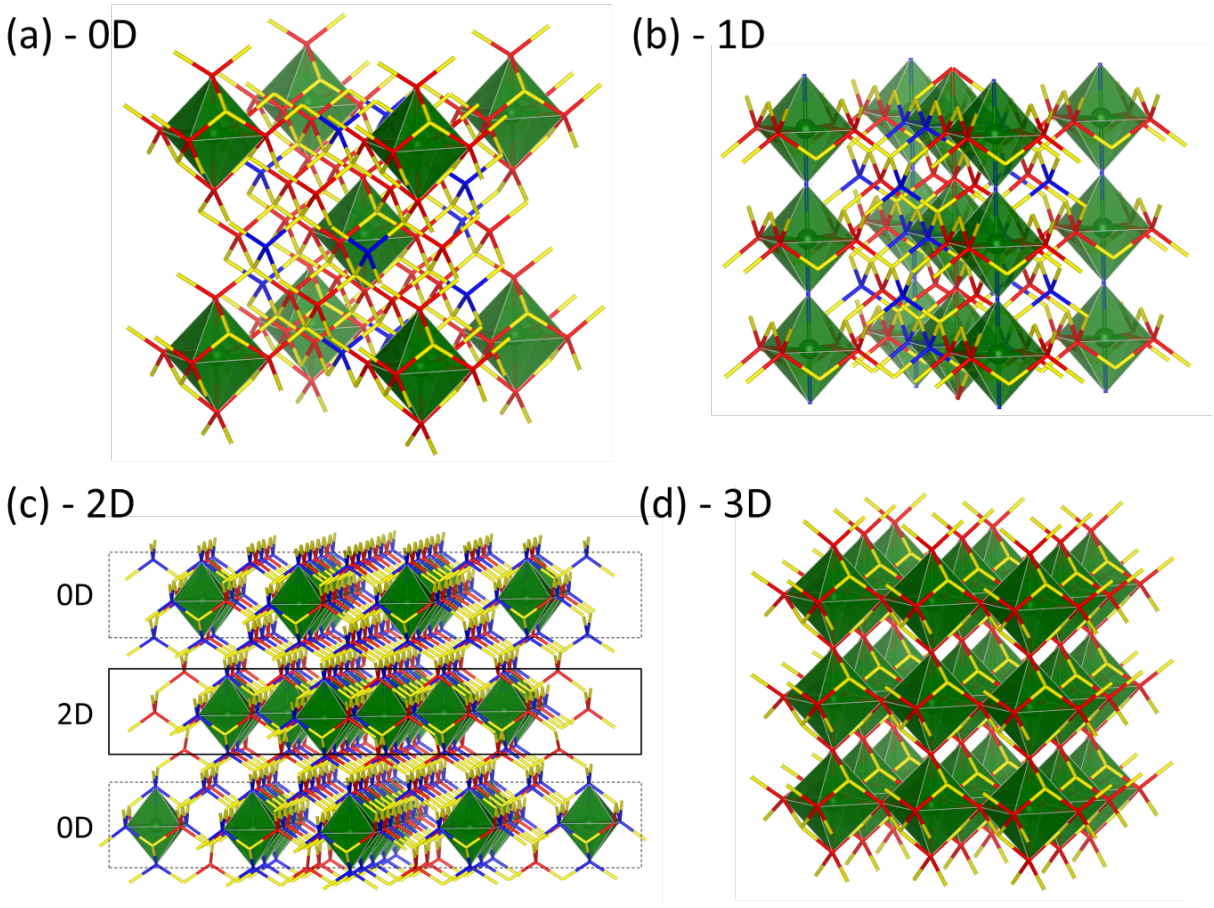

Figure 5 Schematic representations of the crystal structures of (a) the group B colusite $Cu_{26}V_2Sn_2As_4S_{32}$ ($P\bar{4}3n$) and the group C (b) mooihoekite $Cu_9Fe_9S_{16}$ ($P\bar{4}2m$), (c) haycockite $Cu_4Fe_5S_8$ ($P222$), and (d) sulvanite Cu_3VS_4 ($P\bar{4}3m$), showing only the bonds within the "host" structure and the connection dimensionality of the octahedral [TS$_4$]M_6 complexes (in green) for clarity.

A non-exhaustive list of such compounds includes the mineral phases mawsonite $Cu_6Fe_2SnS_8$, catamarcaite Cu_6WGeS_8, omariniite $Cu_8Fe_2ZnGe_2S_{12}$, stannoidite $Cu_8Fe_2ZnSn_2S_{12}$, germanite $Cu_{26}Fe_4Ge_4S_{32}$, talnakhite $Cu_9Fe_8S_{16}$, renierite $Cu_{20}Zn_2Fe_8Ge_4S_{32}$, colusite $Cu_{26}V_2Sn_2As_4S_{32}$ and kiddcreekite Cu_6WSnS_8, Table 2. Note that, among all these phases, only catamarcaite Cu_6WGeS_8 is a derivative of the wurtzite structure (Fig. 3c). Additionally, with the exception of talnakhite, $Cu_9Fe_8S_{16}$, that contains only block *d* metals, most group B mineral phases combine block *d* and *p* elements with a majority of copper atoms. As in group A phases, the block *p* element is always in its d^{10} configuration in the group B phases.

Accepted Manuscript

Table 2 Structural information on group B phases and their corresponding [TS$_4$]M_6 complexes.

Mineral	Composition	Space group	Cell parameters (Å)	Volume (Å^3)	[TS$_4$]M_6	$d_{T\text{-}M}$ (Å)	T/S	□/S	Ref.
mawsonite	$Cu_6Fe_2SnS_8$	$P\bar{4}m2$	a = 7.603 c = 5.358	309.7	[$Fe^{3+}S_4$]Cu_4Fe_2	2.68 (Cu) 2.73 (Fe)	1/8	-	[33]
catamarcaite	Cu_6WGeS_8	$P6_3mc$	a = 7.524 c = 12.390	607.4	[$W^{6+}S_4$]Cu_6	2.73	1/8	1/8	[34]
omariniite	$Cu_8Fe_2ZnGe_2S_{12}$	$I222$	a = 10.774 b = 5.392 c = 16.085	934.5	[$Cu^{+}S_4$]Cu_4Fe_2*	2.70/2.78 (Cu) 2.74 (Fe)	1/12	-	[35]
stannoidite	$Cu_8Fe_2ZnSn_2S_{12}$	$I222$	a = 10.767 b = 5.411 c = 16.118	939.0	[$Cu^{+}S_4$]Cu_4Fe_2*	2.70/2.71 (Cu) 2.74 (Fe)	1/12	-	[36]
germanite	$Cu_{26}Fe_4Ge_4S_{32}$	$P\bar{4}3n$	a = 10.586	1186.4	[$Cu^{+}S_4$]Cu_6*	2.72	1/16	-	[37]
talnakhite	$Cu_9Fe_8S_{16}$	$I\bar{4}3m$	a = 10.593	1188.7	[$Fe^{3+}S_4$]Cu_3Fe_3§	2.72 (Cu/Fe)	1/16	-	[38]
renierite	$Cu_{20}Zn_2Fe_8Ge_4S_{32}$	$P\bar{4}2c$	a = 10.623 c = 10.551	1190.5	[$Fe^{3+}S_4$]Cu_4Fe_2	2.65/2.67 (Cu) 2.81 (Fe)	1/16	-	[39]
colusite	$Cu_{26}V_2Sn_2As_4S_{32}$	$P\bar{4}3n$	a = 10.621	1198.1	[$V^{5+}S_4$]Cu_6	2.73	1/16	-	[40]
kiddcreekite	Cu_6WSnS_8	$F\bar{4}3m$	a = 10.818	1266.0	[$W^{6+}S_4$]Cu_6	2.69	1/8	1/8	[41]

* The cationic distribution in these compounds involves highly unlikely d^{10} interstitial atoms (*i.e.* T = Cu^{+}).
§ Considering the chemical composition of this compound, the presence of Fe^{2+} in the structure (*i.e.* 1 per formula unit) and therefore in the [TS$_4$]M_6 complex cannot be excluded.

The presence of metal atoms in isolated interstitial positions leads to an M_{tot}/S ratio slightly above 1, with once again a couple of exceptions with catamarcaite and kiddcreekite for which the ratio equals to 1. This singularity is caused by an incomplete occupation of the underlying host structure with a number of voids, □, equivalent to the number of interstitial T atoms (Table 2). Note that the nature and oxidation state of the interstitial cations in these phases can vary significantly, *e.g.* elements with formal charges Cu^{+}, Fe^{3+}, V^{5+} or W^{6+}, for natural minerals (Table 2) and can be extended further for synthetic derivatives such as colusites with Ti^{4+}, Nb^{5+}, Ta^{5+}, Cr^{6+} and Mo^{6+} (Fig. 3d). [42–44] It is important to mention that the existence of d^{10} cation Cu^{+} in interstitial position, reported for mineral phases omariniite [35], stannoidite [36] and germanite [37], is questioned, especially for synthetic compounds.[45] The cationic distribution in these structures are worthy of a closer look and a re-investigation is currently on-going for synthetic phase. Conversely, the metal atoms, M, that compose the environment of the interstitial cation, T, in the tetrahedral-octahedral [TS$_4$]M_6 complex, are either exclusively Cu or a combination of Cu and Fe (Table 2). Finally, the observed T-M distances are relatively homogeneous, regardless of the nature or oxidation state of the interstitial cation, suggesting that T-M interactions in these complexes are significant. Overall, because the complexes are isolated from one-another, the crystal chemistry and the electronic structure remains dictated by the tetrahedral sphalerite or wurtzite-type network.

Group C also includes compounds exhibiting a crystal structure derivative of the sphalerite, or wurtzite, and T atoms in "interstitial" position, and consequently, leading to tetrahedral-octahedral [TS$_4$]M_6 complexes (Fig. 2b). However, in group C phases, these tetrahedral-octahedral [TS$_4$]M_6 complexes are connected to one-another in either 1D, 2D or 3D arrangements (Fig. 5b, c, d) while they are isolated (0D) in group B phases.

Accepted Manuscript

This group includes the natural mineral sulvanite Cu_3VS_4, represented in Fig. 2d and Fig. 5d, and its synthetic derivatives Cu_3NbS_4 and Cu_3TaS_4 (Table 3). In these phases, the [*T*S$_4$]*M*$_6$ complexes are connected to one-another by their corners in all three directions giving rise to a 3D arrangement of the complexes. As a consequence, the sulvanite structure can also be described as a 3D perovskite [*T*Cu$_3$] framework of corner-sharing *T*Cu$_6$ octahedra (Fig. 5d), where the S anions are inserted. This 3D arrangement of the [*T*S$_4$]*M*$_6$ complexes is probably responsible for the presence of 1/4 of metallic voids in the sphalerite-type network, explaining the M_{tot}/S ratio equals to 1 (Table 3). This is supported by the crystal structure of the synthetic phase of group C, Cu_4TiS_4, characterised by a 2D arrangement of the [*T*S$_4$]*M*$_6$ complexes, i.e. of the layers of corner-sharing TiCu$_6$ octahedra, resulting in the absence of metallic voids on the sphalerite-type network (Table 3). Indeed, this 2D arrangement of the [*T*S$_4$]*M*$_6$ complexes in Cu_4TiS_4 probably allows to "relax" the constraints generated by the 25% occupation of the interstitial positions with respect to the host structure. Note that the structure of Cu_4TiS_4 is related to that of the sulvanite Cu_3VS_4 by a [½, ½, 0] translation of one layer of tetrahedral-octahedral complexes out of two, leading to a doubling of the *c* parameter and the occurrence of an "additional" Cu atom compared to sulvanite (Table 3). Conversely, the synthetic compound Cu_2WS_4 ($P\bar{4}2m$) and its high-pressure phase ($I\bar{4}2m$) exhibit a metal-poor sulvanite-type structure (Table 3), that can be described as layers of edge-sharing CuS_4 and WS_4 tetrahedra (as in sulvanite) stacked along the *c* axis and separated by Van der Waals gaps (Fig. 2d), giving rise to a 2D arrangement of the complexes. This stacking leads to a bi-dimensional structure composed of corner-sharing tetrahedral-square planar [WS$_4$]Cu$_{4\square 2}$ along the (*a*,*b*) plane (Table 3).

This group also includes the mineral phases mooihoekite $Cu_9Fe_9S_{16}$ and haycockite $Cu_4Fe_5S_8$ (Table 3). The former is composed of 1D isolated chains of corner-sharing tetrahedral-octahedral complexes [*T*S$_4$]*M*$_6$, i.e. of corner sharing *TM*$_6$ octahedra running along the *c* axis (Fig. 5b). The latter can be described as the stacking of twelve wurtzite-type *M*S$_4$ layers along the *c* axis where every third cation layer contains extra "interstitial" Fe atoms, alternating 2D arrangement of the complexes, i.e. edge-sharing CuS_4 and WS_4 tetrahedra layers as observed in the metal-poor sulvanite-type structure of Cu_2WS_4, with group B-like layers of isolated (0D) tetrahedral-octahedral complexes (Fig. 5c and Table 3).

All phases from group C only contain one block *d* element other than Cu. When this element belongs to the first half of block d, meaning that the *d* valence orbitals are less than half-filled, it is the minority cation (Cu/*M* > 1) and its oxidation state is at its maximum (i.e. d^0). If the element belongs to the second half of block *d*, therefore the *d* valence orbitals are more than half-filled and the Cu/*M* ratio can be less than 1, it exhibits an intermediate oxidation state (e.g. Fe^{3+}, d^5). However, to the best of our knowledge, this second case only concerns two ternary sulphides from the Cu-Fe-S system (Table 3) and further investigations into other compounds exhibiting similar crystal structures are welcome. Meanwhile, compounds crystallising in the sulvanite-type structure can accommodate a block *d* element with a broad range of oxidation states (i.e. +IV, +V and +VI) owing to structural alterations in the "Cu-S" network in order to counterbalance the charge. For instance, when V^{5+} is substituted by Ti^{4+}, a structural change in the form of a [½, ½, 0] translation of every second sulvanite-type layer allows for one extra

Accepted Manuscript

Cu^+ per formula unit to be intercalated, forming Cu_4TiS_4. Conversely, when V^{5+} is substituted by W^{6+}, the Cu^+ in (0, 0, ½) position with respect to the sulvanite structure is removed, forming vacant sites between consecutive sulvanite layers (Fig. 2d) and incomplete tetrahedra-octahedral complexes $[WS_4]Cu_4\square_2$ (Table 3). These complexes are thus best described as tetrahedral-square planar $[WS_4]Cu_4$. As it was the case for phases belonging to group B, cations with various oxidation states (Fe^{3+}, Ti^{4+}, V^{5+}, Nb^{5+}, Ta^{5+}, W^{6+}; Table 3) are found in interstitial positions with respect to the host structure. When these cations are at their maximum oxidation state, hence with a d^0 electronic structure, the octahedral environment is solely composed of Cu atoms, either Cu_6 or $Cu_4\square_2$. When the "interstitial" cation is Fe, i.e. not d^0, its chemical surrounding is composed of both Fe and Cu, either Cu_4Fe_2 or Cu_2Fe_4 (Table 3).

Table 3 Structural information on group C phases and their corresponding $[TS_4]M_6$ complexes.

Mineral	Composition	Space group	Cell parameters (Å)	Volume (Å^3)	$[TS_4]M_6$	$d_{T\text{-}M}$ (Å)	T/S	□/S	$[TS_4]M_6$ connexion	Ref.
sulvanite	Cu_3VS_4	$P\bar{4}3m$	a = 5.370	154.9	$[V^{5+}S_4]Cu_6$	-	1/4	1/4	3D	[32]
	Cu_3NbS_4	$P\bar{4}3m$	a = 5.500	166.4	$[Nb^{5+}S_4]Cu_6$	2.75	1/4	1/4	3D	[46]
	Cu_3TaS_4	$P\bar{4}3m$	a = 5.515	167.7	$[Ta^{5+}S_4]Cu_6$	2.76	1/4	1/4	3D	[47]
	Cu_4TiS_4	$I\bar{4}2m$	a = 5.448 c = 10.565	313.6	$[Ti^{4+}S_4]Cu_6$	2.72/2.75	1/4	-	2D	[48]
	$Cu_2\square WS_4$	$P\bar{4}2m$	a = 5.424 c = 5.234	154.0	$[W^{6+}S_4]Cu_4\square_2$	2.71	1/4	1/2	2D	[49]
	$Cu_2\square WS_4$	$I\bar{4}2m$	a = 5.444 c = 10.069	298.4	$[W^{6+}S_4]Cu_4\square_2$	2.72	1/4	1/2	2D	[50]
mooihoekite	$Cu_9Fe_9S_{16}$	$P\bar{4}2m$	a = 10.585 c = 5.383	603.1	$[Fe^{3+}S_4]Cu_4Fe_2$*	2.73 (Cu) 2.69 (Fe)	1/8	-	1D	[51]
					$[Fe^{3+}S_4]Cu_2Fe_4$*	2.69 (Fe) 2.73 (Cu)				
haycockite	$Cu_4Fe_5S_8$	$P222$	a = 10.705 b = 10.734 c = 31.630	3634.5	$[Fe^{3+}S_4]Cu_2Fe_4$§	2.67/2.69 (Cu) 2.67/2.69 (Fe)	1/8	-	2D and 0D	[52]
					$[Fe^{3+}S_4]Cu_2Fe_4$§	2.67/2.69 (Cu) 2.66/2.69 (Fe)				
					$[Fe^{3+}S_4]Cu_2Fe_4$§	2.75 (Cu) 2.72/2.74 (Fe)				
					$[Fe^{3+}S_4]Cu_2Fe_4$§	2.60 (Cu) 2.59/2.72 (Fe)				
					$[Fe^{3+}S_4]Cu_2Fe_4$§	2.68 (Cu) 2.71/2.72 (Fe)				
					$[Fe^{3+}S_4]Cu_2Fe_4$§	2.66 (Cu) 2.72/2.72 (Fe)				

*, § Owing to the chemical formula of these compounds, the presence of Fe^{2+} (i.e. * 4 per formula unit and § 3 per formula unit) in the structure and thus in $[TS_4]M_6$ complexes cannot be excluded.

Accepted Manuscript

Are found in **group D**, compounds characterised by a 3D arrangement of edge-sharing MS_4 tetrahedra, *i.e.* interpenetration of two corner-sharing MS_4 tetrahedra networks (Fig. 2e), thus derived from the anti-fluoride structure, a face-centred cubic network of sulphur where all tetrahedral sites are occupied by metal atoms. This group includes the high-temperature phases of some minerals such as bornite Cu_5FeS_4 ($Fm\bar{3}m$, a = 5.50 Å and V = 166.4 Å^3 [53]), digenite $Cu_{1.8}S$ ($Fm\bar{3}m$, a = 5.564 Å and V = 172.3 Å^3 [54]), and stromeyerite AgCuS ($Fm\bar{3}m$, a = 5.956 Å and V = 211.3 Å^3 [55]). These two former phases, high-temperature bornite and digenite, are characterised by a partial occupation of all cationic sites while intermediate phases occur at medium and low-temperatures for bornite, cubic ($Fm\bar{3}m$, a = 10.981 Å and V = 1324.0 Å^3 [56]) and orthorhombic ($Pbca$, a = 10.950 Å, b = 21.862 Å and c = 10.950 Å and V = 2621.3 Å^3 [57]). These phases crystallise in an array of antifluoride and sphalerite-type sub-lattices forming a face-centred cubic network of sulphur atoms in which half of the tetrahedral sites are occupied, in an ordered fashion, by metal atoms. Compounds found in this group D all exhibit a cationic sub-lattice mainly composed of univalent copper or silver ([Cu, Ag]/$M \geq 5$), Cu(I) or Ag(I), along with block *d* transition metals, and are characterised by a high M_{tot}/S ratio, between 1.5 and 2.

Finally, **group E** includes all the remaining compounds exhibiting at least one polyhedron with a metal coordination other than tetrahedral. This different chemical surrounding is caused either by the presence of elements that cannot accommodate a tetrahedral coordination of sulphur such as block *s* and block *f* metals, by very important local disorder, or by a smaller proportion of monovalent Cu^+ compared with compounds from the previous groups. Consequently, this group E includes a large number of inorganic copper-based sulphides. Nevertheless, for coherency with compounds of the groups A to D, only phases composed of block *d* metals and/or block *p* elements for which ionic Shannon radius and electronegativity are equivalent to those of univalent Cu(I), will be discussed in the following section.
Therefore, this group includes numerous *p*-type materials such as $CuCrS_2$ ($R3m$, a = 3.482 Å, c = 18.686 Å and V = 196.2 Å^3 [58]), composed of CuS_4 tetrahedra sharing a face with CrS_6 octahedra and giving rise to relatively short Cu-Cr distances (2.77 Å), Cu_4SnS_4 ($Pnma$, a = 13.566 Å, b = 7.689 Å, c = 6.416 Å and V = 669.4 Å^3), composed of CuS_3 trigonal planar, and SnS_4 and CuS_4 tetrahedra,[59] and tetrahedrite $Cu_{12}Sb_4S_{13}$ ($I\bar{4}3m$, a = 10.391 Å and V = 1121.9 Å^3 [60]), composed of trigonal planar CuS_3, CuS_4 tetrahedra and $SbS_3\square$ pseudo-tetrahedra, where □ is the Sb^{3+} lone pair. [61] Note that Cu_4SnS_4 and $Cu_{12}Sb_4S_{13}$ are both characterised by a structural transition at low temperature leading to lower symmetry crystal structures.[59,62,63] The room temperature crystal structure of Cu_4SnS_4 is characterised by local disorder on the copper framework, *i.e.* splitting into three positions of two thirds of the copper sites, leading to the displacement of copper atoms towards the faces of the tetrahedron, and consequently, to the existence of trigonal planar CuS_3.[59] The room temperature crystal structure of tetrahedrite, shown in Fig. 6a, is a derivative of the sphalerite-type structure and closely related to that of the group B talnakhite $Cu_9Fe_8S_{16}$ ($I\bar{4}3m$, a = 10.593 Å and V = 1188.7 Å^3 [38]) with a few differences: (i) tetrahedrite exhibits a defect anionic sublattice with a vacancy on the 8*e* site

Accepted Manuscript

and (ii) sulphur atoms are found in the interstitial position 2*a*. [38] These differences in the sphalerite-type sublattice of tetrahedrite give rise to (i) a trigonal planar coordination around the Cu(12*e*) atoms (Fig. 6b) and (ii) the absence of tetrahedral-octahedral complexes $[TS_4]M_6$. These specific features are the reasons why Cu_4SnS_4 and tetrahedrite $Cu_{12}Sb_4S_{13}$ are group E copper sulphides despite a majority of univalent Cu(I) (Cu/*M* = 4 and 3, respectively). Note that Cu_4SnS_4, tetrahedrite and talnakhite, despite the aforementioned differences, exhibit extremely low thermal conductivity.[59,61,62,64,65]

The group E also includes *n*-type compounds (Cu/*M* < 1) such as thiospinel $Cu_2CoTi_3S_8$ ($Fd\bar{3}m$, a = 9.885 Å and V = 966.0 Å^3 [66]), containing CuS_4 tetrahedra and (Ti,Co)S_6 octahedra, and the synthetic phase $Cu_4Sn_7S_{16}$ ($R\bar{3}m$, a = 7.372 Å, c = 36.010 Å and V = 1694.8 Å^3 [67]), containing CuS_6 and SnS_6 octahedra and CuS_4 tetrahedra, some of them leaning strongly toward a CuS_3 trigonal planar coordination (Fig. 6c). Essentially, the crystal structure of $Cu_4Sn_7S_{16}$ can be described as a defect (thio)spinel AB_2X_4 (unit cell parameter a' ≈ 10.40 Å) with a unit cell parameter relationship: $a = b = a'\sqrt{2}/2$ et $c = 2a'/\sqrt{3}$. This structural transformation from a cubic to a rhombohedral unit cell generates two non-equivalent 6*c* sites in the $Cu_4Sn_7S_{16}$ structure. These two sites replace the tetrahedral sites of the (thio)spinel structure and are respectively fully occupied or half-filled by Cu atoms. In the (thio)spinel structure, the octahedral site is divided into 3 sites, 18*h*, 3*b* and 3*a*, fully occupied in the $Cu_4Sn_7S_{16}$ structure by Sn for the 18*h* and 3*b* sites, and by Cu for the 3*a* site. The $Cu_4Sn_7S_{16}$ structure is completed by four non-equivalent sites, 18*h*, 18*h*, 6*c* and 6*c*, all nearly fully occupied by sulphur atoms. Overall, in the $Cu_4Sn_7S_{16}$ crystal structure, 3/4 of the tetrahedral sites are occupied by Cu, the remaining 1/4 are vacancies, while 1/8 and 7/8 of octahedral sites are respectively occupied by Cu and Sn. $Cu_4Sn_7S_{16}$ can thus be considered as a defect thiospinel with chemical formula $(Cu_{0.75}\square_{0.25})(Sn_{1.75}Cu_{0.25})S_4$. [67,68] Note that, similarly to tetrahedrite and talnakhite, the complex crystal structure of $Cu_4Sn_7S_{16}$ leads to extremely low thermal conductivity. [67,68]

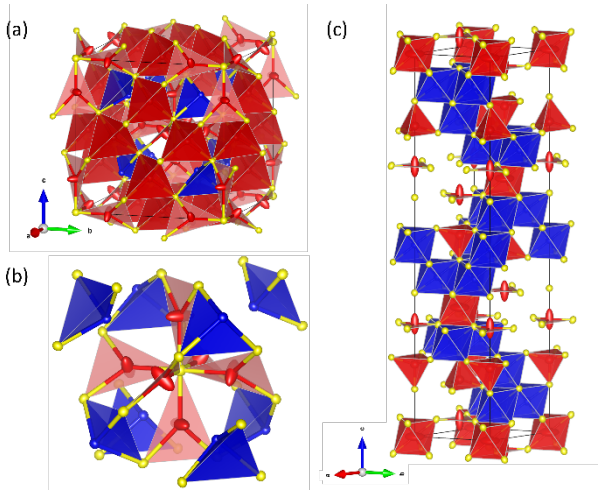

Figure 6 Schematic representations of the crystal structure of group E copper sulphides (a) tetrahedrite $Cu_{12}Sb_4S_{13}$ ($I\bar{4}3m$) with (b) its characteristic central S atom (in yellow) in an octahedral coordination of trigonal planar CuS_3 and (c) $Cu_4Sn_7S_{16}$ ($R\bar{3}m$). All representations

Accepted Manuscript

highlight the large anisotropic thermal displacement of the Cu atoms (in red) across the CuS_3 trigonal plans.

3. Structure-properties relationship in inorganic copper sulphides

The transport properties of complex copper sulphides have been the subject of detailed investigations, in particular for thermoelectric and photovoltaic applications. In recent years, researchers have focused on the structure-properties relationships and this strategy is paying off with complex copper sulphides now exhibiting high TE performances. A non-exhaustive list of some of these copper sulphides and their respective figure of merit, *ZT*, are displayed in Fig. 7.[27,31,43–45,68–88] From this figure, one can note that two families stand out by their performances approaching a figure of merit of 1, *i.e.* tetrahedrites and colusites,[10,11] owing to the very low thermal conductivities caused by their complex crystal structure classified in group E and B, respectively. In group B, the complexity arises from the large unit cells with cationic disorder while group E compounds exhibit high anisotropic atomic vibrations. These structural features can be used to engineer good thermoelectric materials by adjusting both electrical and thermal transport properties. In photovoltaic applications, the potential of a solar cell device is illustrated by the light-to-electricity conversion efficiency (theoretically limited at ~34% for a single-junction according to the Shockley-Queisser model) and fill factor (typically ranging from 50% to 80%). Efficient solar absorber materials typically exhibit optical band gaps around 1.0-1.5 eV and large light absorption coefficients (> 10^4 cm^{-1}). Ternary and quaternary copper sulphides now exhibit promising conversion efficiencies, around 10-15 % for members of group A such as copper tin sulphide (CTS), copper indium gallium sulphide (CIGS) and kesterite/stannite Cu_2MSnS_4 (*M* = divalent cation) phases.[89,90]

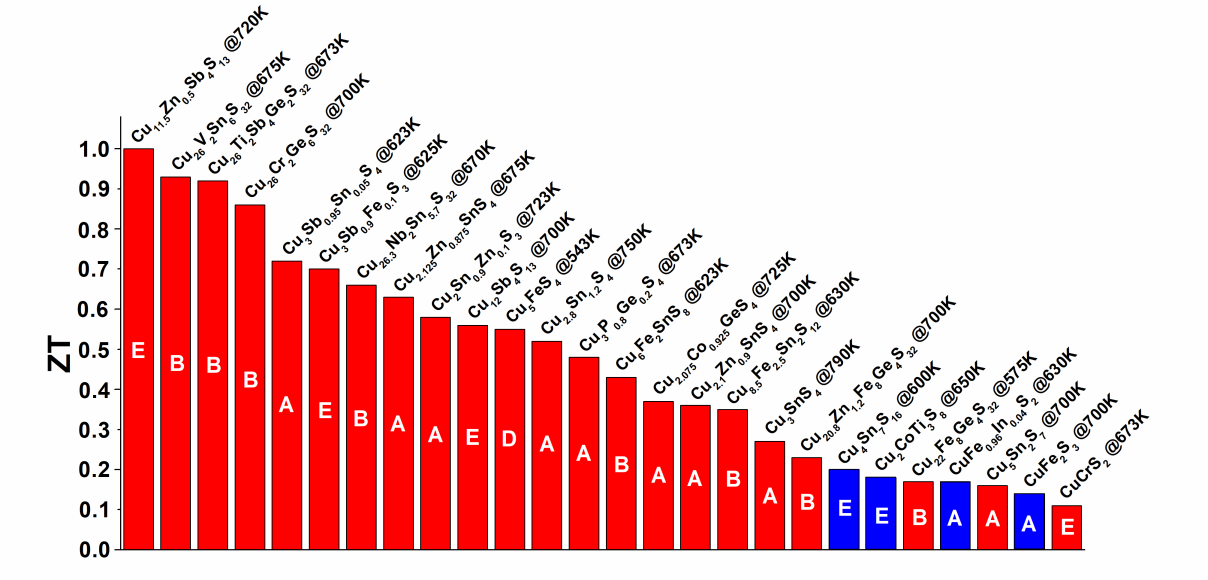

Figure 7 Classification of ternary and quaternary copper sulphides (*p*-type in red, *n*-type in blue) depending on their figure of merit, *ZT*. [27,31,43,45,68–88] The list is not exhaustive and includes only samples with extensive crystal structure analysis. The compounds belong to the groups indicated in the column.

Accepted Manuscript

10.1002/anie.202108686

Of note, copper sulphides include both *n*- and *p*-type materials (Fig. 7), depending on the nature of the main charge carriers and intimately linked to the Cu/*M* ratio (Fig. 8). Indeed, when this ratio is below 1, the main charge carriers are electrons and the material is *n*-type. Conversely, a Cu/*M* ratio over 1 typically yields materials with *p*-type conduction. When the ratio is equal to 1, both *n*- and *p*-type materials can be obtained. This feature helps to explain the crystal chemistry of copper sulphides that, when dominated by a majority of univalent copper (*i.e.* Cu/*M* over 1) in tetrahedral coordination of sulphur, leads to a strong hybridisation of the Cu 3*d* and S 3*p* orbitals, allowing holes to be delocalised.[91] Other metal atoms can act as a charge reservoir (holes donor or acceptor) for the conductive "Cu-S" network that indirectly adopts a Cu(I)-Cu(II) mixed valence.[92] Conversely, when the phase is mainly composed of metal elements other than copper (*i.e.* Cu/*M* below 1), the Fermi level is located near or within the conduction band. For example, in Fe-rich compounds, the Fe 3*d* states play a crucial role in contributing to the electronic band structure of these *n*-type materials,[71] while in *p*-type stannoidite, the transport properties remain governed by the Cu-S network.[74] These differences in band structures and conduction mechanisms are driven by the contrasts in chemical bonding between block *d* transition metals and block *p* elements when associated with sulphur (Fig. 4).

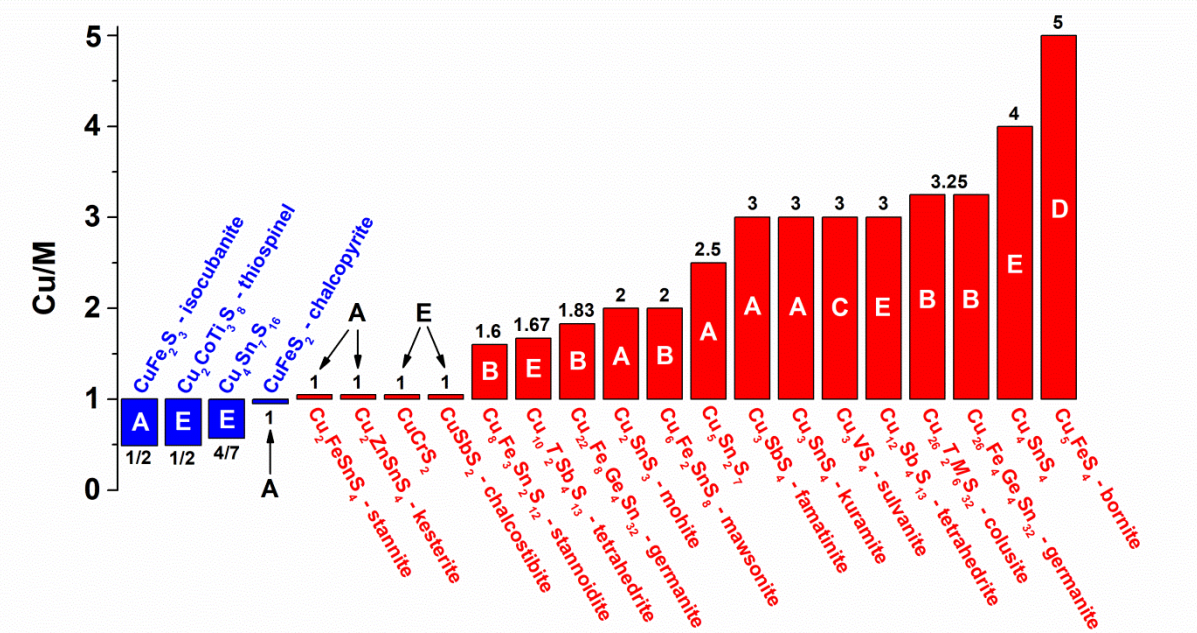

Figure 8 Classification of ternary and quaternary copper sulphides depending on their Cu/*M* (where $M \neq$ Cu) ratio showing the influence on this ratio over the nature of the main charge carriers (*p*-type in red, *n*-type in blue). The compounds belong to the groups indicated in the column.

In this section, we will look at each group and focus on the impact of interesting structural characteristics on the transport properties. Although the most promising TE materials will be discussed, this work does not constitute an extensive review of the current state-of-the-art copper sulphides for thermoelectric or photovoltaic applications. Instead, we aim at providing

Accepted Manuscript

key information of the structure-properties relationships that can be used as a toolbox for the identification and optimisation of future materials for energy harvesting.

The **group A** is the simplest in term of crystal structure with only corner-sharing tetrahedra with a significant portion of CuS_4 tetrahedra. Whether they form a sphalerite-type or a wurtzite-type array of tetrahedra, the electronic band structure of the materials are relatively similar with the top of the valence band being mainly composed of Cu 3*d* and S 3*p* orbitals. In *p*-type ternary and quaternary copper sulphides, thus not limited to group A compounds, this feature leads to the formation of a "Cu-S" conductive network. [91] The Cu/*M* ratio and the oxidation state of the other cations then determine the proportion of divalent copper in this conductive network. This is the concept of "Cu(I)-Cu(II)" copper mixed valence in thermoelectric copper sulphides, resembling that of "Cu(II)-Cu(III)" in superconducting cuprates. [92] Note that static Cu^{2+} do not occur in sulphides with the exception of CuS. The presence of the Cu(I)-Cu(II) mixed valence, however, is undeniable and forms the basis of hole doping in thermoelectric sulphides, with a high proportion of "mobile" divalent copper being achievable.
As this concept holds for all five groups of *p*-type copper sulphides described here, it provides a strong basis for the engineering of materials with specific transport properties. In fact, the tetrahedral framework of CuS_4, whether the researchers are purposely looking for a "Cu-S" conductive network or not, is considered as a solid starting point for the identification of new thermoelectric materials.[5,73,82] Group A thus includes many performing thermoelectric materials despite the "simple" nature of their crystal structure and the rather high thermal conductivities that are often associated with it (Fig. 9). Unsurprisingly, the best performing group A thermoelectric materials involve extrinsic effects that hinder the thermal diffusivity, such as nanostructuring or multi-phases synthesis for the very promising mohite family, Cu_2SnS_3 (CTS). [93–96] The best performances so far among all group A compounds, with a maximum *ZT* value of *ca*. 0.85 at 723 K, have been achieved for the composition $Cu_2Sn_{0.8}Co_{0.2}S_3$, containing a mixture of sphalerite-type cubic (space group $F\bar{4}3m$), tetragonal (space group $I\bar{4}2m$) and monoclinic Cu_2SnS_3 (space group Cc) phases. [93] CTS offer additional prospects owing to the number of phases with different crystal structures that are obtained around the prototypical composition Cu_2SnS_3. The change of the Cu/Sn ratio modifies the cationic ordering and leads to the formation of different structures. In the series $Cu_{2+x}Sn_{1-x}S_3$, monoclinic Cc is obtained for x = 0 (Cu_2SnS_3), cubic $P\bar{4}3n$ with mixed occupancy for x = 0.063 ($Cu_{22}Sn_{10}S_{32}$), or monoclinic $C2$ for x = 0.143 ($Cu_5Sn_2S_7$).[27,97] The composition, cationic ordering and/or disordering phenomena observed in those different phases strongly affect the carrier concentration and mobility, as well as phonon scattering, and final thermoelectric performances. [27,82]
In comparison, the related sphalerite-type tetragonal chalcopyrite $CuFeS_2$ [72,98] and cubic isocubanite, $CuFe_2S_3$, [76] exhibit a relatively high thermal conductivity (Fig. 9) that results in *ZT* values below 0.3 at 673 K. [76] Note that because the Cu/*M* ratio is below 1, chalcopyrite and isocubanite are *n*-type materials but the valence band remains mainly composed of Cu 3*d* and S 3*p* orbitals. As for mohite derivatives, simple doping strategies have been shown to be

Accepted Manuscript

successful in chalcopyrite,[98] isocubanite,[76] kesterite Cu_2ZnSnS_4 [81], stannite Cu_2FeSnS_4[99] and famatinite. [100]

Most of the performing materials for photovoltaic application are also sphalerite-derivative compounds from group A. Among these widely studied materials, copper tin sulphides (CTS) and kesterite Cu_2ZnSnS_4 (CZTS) phases are considered very promising due to their efficiency and constituting non-toxic, low-cost and earth-abundant elements. [12,14,15,17] Their structural proximity with the toxic but very efficient $Cu_2(In, Ga)Se_4$ (CIGS) leads to similar performances and key characteristics such as a direct band gap (1–1.5 eV), high absorbance coefficient and *p*-type conductivity. [17] CTZS can thus reach a power conversion efficiency (PCE) up to 9.2%. [101] One issue that has so far hindered the wide-scale application of group A photovoltaics is the difficulty to prepare thin-films without significant defects or impurities. Similarly, the indium-containing ternary, $CuInS_2$ (CIS) exhibits a good PCE of 11.4%, [102] however, the cost and scarcity of indium is a concern for large-scale application. Alternatively and despite lower performances than CZTS, CTS offers additional prospects owing to the number of phases with different crystal structures that are obtained around the prototypical composition Cu_2SnS_3. These cubic, tetragonal or monoclinic phases have different band gaps that can be adjusted through doping or control of the Cu/Sn ratio. Finally, considering the recent efforts that have been made in order to identify new crystal structures in the Cu-Sn-S family, [27,82] research on CTS photovoltaics remains very promising.

In the wurtzite-type system, derivatives from the mineral enargite, Cu_3PS_4, are attracting attention as potential candidates for both thermoelectric and photovoltaic applications. [83,103] The multi-band characteristics of the valence band, similar to what has been reported for sphalerite-type structures, yields heavy charge carriers effective masses and good electrical performances. Maximum power factor values between 0.4 mW m^{-1} K^{-2} and 0.8 mW m^{-1} K^{-2} at around 700 K have been reported depending on the concentration of Ge dopant. [83] Because of grain boundary scattering from the nano-sized crystallites, the thermal conductivity remained low and the resulting *ZT* reached 0.5 at 673 K. While currently under-investigated, complex copper sulphides derivatives of the wurtzite-type system definitely offer some interesting prospects for cost-efficient thermoelectric materials engineering.

Accepted Manuscript

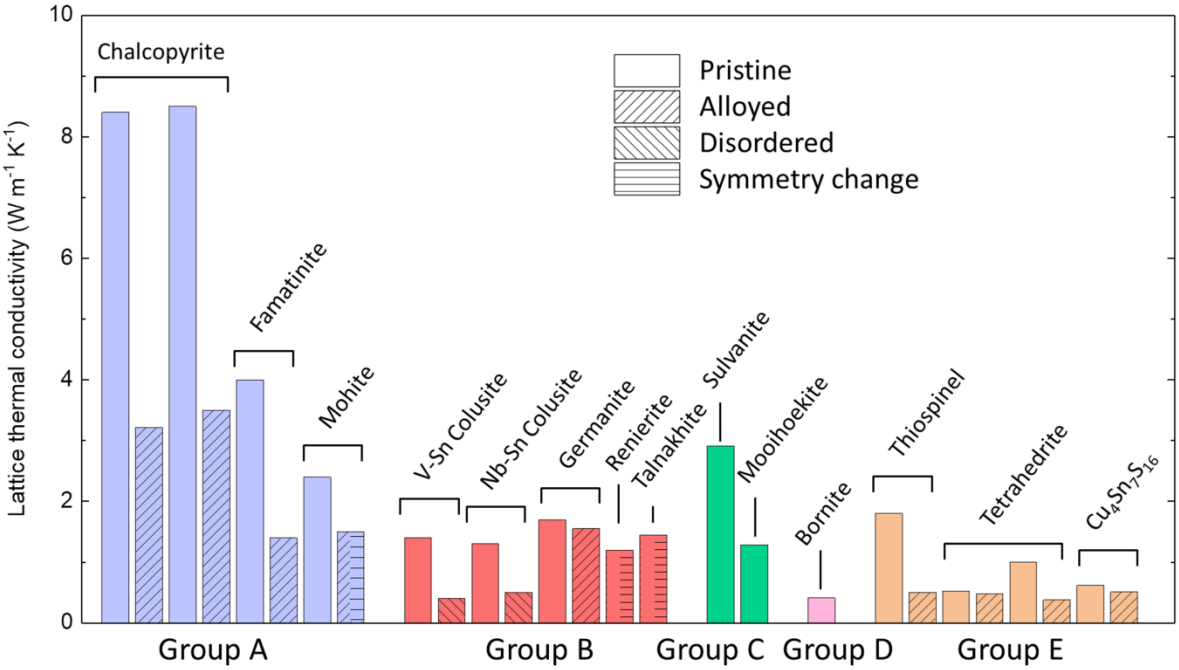

Figure 9 Reported lattice contribution to the thermal conductivity at room temperature for a few representative materials of each group. [45,65,72,77,78,80,88,98,104–109]

Materials belonging to the **group B** share many characteristics with group A compounds because of their structural proximity, as described in the previous section, with a similar electronic structure. The multiband character of the top of the valence band, mainly composed of Cu 3*d* and S 3*p* orbitals, and the resulting "Cu-S" conductive network is retained. This allows group B materials to exhibit similarly interesting and promising electrical transport properties. [7,43,74,77,110–112] However, the addition of an "interstitial" atom and the resulting changes in the crystal structure is very consequential in term of performances.[7,91] First of all, the unit cell can be significantly enlarged to include the new elements in specific crystallographic sites. Large unit cells, combined with at least two dissimilar cations on similar crystal sites, usually yields lower thermal conductivities than observed for group A sulphides (Fig. 9).[65] In some instances, the long-range ordering of the cations belonging to the host structure can be disturbed through temperature-induced sulphur volatilisation or cation off-stoichiometry, resulting in an even lower thermal conductivity (Fig. 9).[78,80,113,114] For instance, because the "Cu-S" conductive network is mostly preserved and the thermal conductivity significantly altered in the synthetic colusite $Cu_{26}V_2Sn_6S_{32}$, the overall performance can be dramatically improved with a maximum *ZT* above 0.9 at 673 K.[78]

The most important feature that surfaces with the addition of "interstitial" cations is the formation of a tetrahedral-octahedral [*T*S$_4$]*M*$_6$ complex (Fig. 2b). This complex, resulting from the short contacts between the "interstitial" *T* cation and the surrounding *M* atoms (*M* = Cu, Fe, Table 2), has a dramatic impact on the transport properties of the materials. The presence of unconventional *T*-Cu bonds which enhance dramatically the power factor of these sulphides clearly confirms that the chemical bonding perspective developed by Wuttig *et al*., [115,116] Kanadzidis *et al*.[117] and Biswas *et al*.[118] is a very promising approach for designing superior

Accepted Manuscript

thermoelectrics. The complexes impact on the transport properties through their remote action on the symmetry of the surrounding tetrahedra that belong to the conductive network. [119] Therefore, the symmetry and nature of these complexes should be carefully investigated when engineering new materials for energy production. In the high-performance Cr-Ge colusite, $Cu_{26}Cr_2Ge_6S_{32}$, an exceptionally high power factor ranging between ≈1.9 mW m^{-1} K^{-2} and 1.94 mW m^{-1} K^{-2} at temperatures comprised between 500 K and 700 K was reported.[43] The investigation concluded that the occupation of the "interstitial" site by the smaller, more electronegative Cr^{6+} cation, compared with other group 6 elements, led to a lesser distortion of the conductive Cu-S network while modifying metallicity due to the particular nature of Cr-Cu interactions. The resulting *ZT* value of 0.86 at 700 K is among the highest reported for a complex copper sulphide. The impact of the "interstitial" cation on the transport properties was later confirmed with the added notion of cation-size mismatch when the interstitial site was statistically occupied by two dissimilar cations.[119] The consequence of such cationic disorder in the "interstitial" position is a clear change of conduction mechanism in the materials, as demonstrated by low-temperature transport properties measurements, from a typical acoustic phonon scattering to an ionised impurity-like scattering mechanism. A similar change is also achieved by providing the structure with extra cations in order to statistically occupy the interstitial tetrahedral sites not belonging to the superstructure position.[113] In addition, $Cu_{26}Ti_2Sb_6S_{32}$, the first semiconducting compound with the colusite structure, exhibits an intrinsically low lattice thermal conductivity ranging between 1.6 W K^{-1} m^{-1} at 300 K and 0.6 W K^{-1} m^{-1} at 673 K.[44] High-performance *TE* properties can be achieved by partial Ge for Sb substitution reaching *ZT* value of 0.9 at 673K. [44] From these recent investigations on colusites, it appears that the *T* site is only occupied by a d^0 cation (Ti^{4+}, V^{5+}, Nb^{5+}, Ta^{5+}, Cr^{6+}, Mo^{6+}, W^{6+}), whereas the associated *M* site is occupied by a cation with a d^{10} configuration similar to Cu^+ (*M* =Ge^{4+}, Sn^{4+}, Sb^{5+}) exclusively.[7,44] This feature is governed by the particular nature of the *T*-Cu bond in the complex $[TS_4]Cu_6$, that is ensured by the *d-d* overlapping of the orbitals of the acceptor d^0 *T* cations and donor d^{10} Cu^+ cations respectively.

These findings demonstrate the importance of interstitial cations in every complex copper sulphide exhibiting a structure derived from an ordered sphalerite-type arrangement. Promising performances have also been reported in other families belonging to group B such as talnakhite $Cu_{17.6}Fe_{17.6}S_{32}$, with a *ZT* of 0.23 at 625 K,[65] germanite $Cu_{22}Fe_8Ge_4S_{32}$ with a *ZT* of 0.27 at 700 K, [120] stannoidite $Cu_8Fe_3Sn_2S_{12}$ with a *ZT* of 0.35 at 630 K[74] and a *ZT* predicted to reach around 0.5 at 800 K for doped mawsonite $Cu_6Fe_2SnS_8$. [112] Interestingly, talnakhite and renierite, two phases structurally closely related from group A chalcopyrite and group B germanite respectively, both exhibit very low lattice thermal conductivity as a result of their complex crystal structure (Fig. 9, Table 1 and 2). These suggest that novel materials are yet to be engineered around prototypical compositions of group A and B compounds.

In comparison with the aforementioned compounds, materials characterised by a connectivity of tetrahedral-octahedral $[TS_4]M_6$ complex (from 1D to 3D), as those derived from the sulvanite-type structure and belonging to **group C** (Table 3) have attracted moderate attention for their transport properties. The semiconducting sulvanite, Cu_3VS_4, does have a band gap

Accepted Manuscript

suitable for photovoltaic applications but also a heavier hole effective mass compared to the Se and Te counterparts. [121] Similarly, little has been done in term of thermoelectric optimisations for the parent sulvanite and the group 5 counterparts Cu_3TS_4, (T = Ta, Nb). The presence of a large number of tetrahedral-octahedral complexes in sulvanite-type Cu_3TS_4, (T = V, Ta, Nb) and the structure that can be regarded as an incomplete sphalerite-type host-structure lead to rather large vacancies that ultimately provide a pathway for ion intercalation. [122] Materials derived from the sulvanite-type structure might therefore be more suitable for applications involving intercalation-deintercalation reactions, such as Li-ion or Na-ion batteries. [123] To the best of our knowledge, the group C material exhibiting the best thermoelectric properties is mooihoekite, $Cu_9Fe_9S_{16}$, with a *ZT* reaching 0.21 at 800 K. [107] Unlike sulvanite, the crystal structure of mooihoekite (Fig. 5b) involves a complete sphalerite "host" that enables mooihoekite to retain good electrical performances. In the same time, the lattice thermal conductivity is two to five times lower than other ternary Cu-Fe-S compounds depending on the temperature. Owing to the rigid chemical bonding in mooihoekite, the reason behind the low thermal conductivity seems to be a larger concentration of grain boundaries. [107] This demonstrates that good *TE* performances can be achieved in complex copper sulphides retaining a "Cu-S" conductive network despite a rigid chemical bonding, provided that extrinsic effects lower the thermal conductivity. Materials derived from structures like that of haycockite might offer some interesting prospects in thermoelectricity.

Interesting thermoelectric performances have been reported for some **group D** materials, in particular around the digenite $Cu_{1.8}S$ and bornite Cu_5FeS_4, phases. The former has been widely investigated with reported *ZT* values well over unity,[124] however, the liquid-like nature of the cation sublattice render them unusable for TE applications, owing to the crippling ionic mobility.[125] While it is still be possible to consider these phases for *TE* applications, detailed investigations often conclude that good performances arise from the combination of holes and ions as charge carriers. Solving the stability issue would thus result in a loss of performances from the specific "liquid-like" character of the sublattice.[125] Materials derived from the mineral bornite, Cu_5FeS_4, do offer a route to supress ionic conductivity using the pinning effect of Fe in "interstitial" position.[126] Although bornite undergoes phase transitions with temperature, thus making it difficult to be used in *TE* devices, it does offer some prospects with *ZT* now reaching values up to 0.8 at 550 K for a readily scalable cost-efficient material. [70,127]

Accepted Manuscript

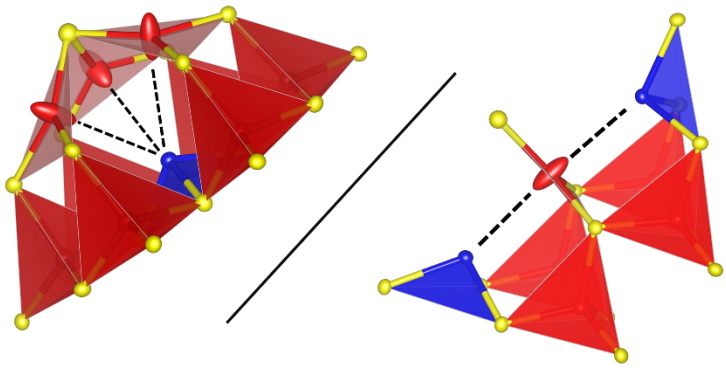

Figure 10 Schematic representations of the trigonal planar coordination of Cu (in red) in tetrahedrite, showing the interaction with lone-pairs of Sb (in blue) and the resulting large anisotropic, out-of-plane, thermal displacement.

Finally, materials from **group E** have shown some excellent, both *n*- and *p*-type, thermoelectric performances owing to the high concentration of consequential structural features.[8,128] In particular, the well-known mineral tetrahedrite has been studied extensively,[129] exhibiting high *ZT* near unity at temperatures below 700 K.[109] In tetrahedrite, $Cu_{12}Sb_4S_{13}$, three structural blocks combine for interesting performances, a sphalerite-type sublattice of CuS_4 tetrahedra that ensures a "Cu-S" conductive network, a CuS_3 trigonal planar unit and a SbS_3 trigonal pyramid (Fig. 10) that both contribute to lowering the thermal conductivity (Fig. 9). The question has been raised whether Sb interacts through a weak bonding (bond order ≈ 0.1) with Cu in trigonal planar position sufficiently in order to promote out-of-plane vibration, [61] or whether Sb simply forms a lone-pair that only mildly impacts the rattling of the copper atoms.[130] In the first case, Cu-Sb interactions effectively modify the CuS_3 trigonal plan and form a $Sb[CuS_3]Sb$ trigonal bipyramid, acting as a large atomic cage that generates a rattling effect. The Cu-Sb interaction thus alternates between weak covalent binding and Sb lone-pair, with a configuration switching back and forth between SbS_3 trigonal pyramid and S_3SbCu_3 trigonal antiprism.[8,61] Therefore, Cu in trigonal planar can alternatively be described as dynamically occupying two out-of-plane positions on each side of the S_3 plan. In a second scenario supported by inelastic neutron scattering, where Cu retains a large anisotropic atomic displacement parameter (ADP) with no significant bonding with the neighbouring Sb, the rattling occurs as a result of the chemical pressure exerted by the trigonal planar environment.[130] This suggests that increasing that chemical pressure through appropriate chemical substitution might lead to an increase in the rattling amplitude and a larger anharmonicity of the Cu vibration. Concomitantly, a larger rattling could interact with the neighbouring metalloid lone pair. In all cases, the presence of a large anisotropic ADP for Cu in trigonal planar (Fig. 6b and 10) and the potential dynamic interactions with the neighbouring metalloids directly impacts the lattice thermal conductivity (Fig. 9). Overall, these characteristic structural features lead to strong bonding anharmonicity and quasilocalised rattling modes that, regardless of their exact nature, help to reduce the lattice contribution to thermal conductivity dramatically by flattening the heat-carrying acoustic phonon branch. [61]

Accepted Manuscript

The downside of this part-crystalline part-liquid state of some of the Cu atoms in tetrahedrite can cause potential issues with ionic conductivity when Cu is found in slight excess. Indeed, in-situ neutron diffraction analysis provided evidence for the co-existence of two tetrahedrite phase with either Cu under- or over-stoichiometry. The two phases coalesce at high temperature demonstrating the mobility of copper above temperatures as low as 393 K. [64] Beyond thermoelectricity, tetrahedrite was also found to be of potential interest for thin-film photovoltaic cells. [131] The overlooked compound Cu_4SnS_4 is another interesting group E that displays high Seebeck coefficient and a very low thermal conductivity owing to compressed acoustic phonon branches in the low-frequency region.[62] This phase exhibits a complex, highly disordered centrosymmetric structure at room temperature and a low-temperature phase transition that changes the transport properties.[62,132] Further investigations into this system are encouraged and expected to yield good results. Some materials from group E are also considered as very attractive for photovoltaic applications. This is for example the case of the $CIGS_4$-$CIGS_7$ compounds, copper-deficient chalcopyrite derivatives, reported to be *p*-type semi-conductors in spite of their Cu/*M* ratio well below unity (*i.e.* < 0.3).[133] This latter point can be explained by the marked 2D character of their crystal structures with a van der Waals gap that singularly contrasts with the 3D character of the group A chalcopyrite crystal structure.[133]

The chemistry of complex copper sulphides for thermoelectric applications is still dominated by *p*-type materials and the overall performance and abundance of *n*-type candidates remains much lower. However, the group E *n*-type $Cu_4Sn_7S_{16}$ offers some interesting prospects with reasonable thermoelectric performances, ZT = 0.2 above 600 K, mainly arising from an intrinsically low thermal conductivity (Fig. 9). [68,134,135] The parallel with tetrahedrite is easily drawn as $Cu_4Sn_7S_{16}$ possesses similar trigonal planar CuS_3 units with strong anisotropic ADP (Fig. 6c). The presence of both octahedra and tetrahedra, as opposed to an array of tetrahedra, contrasts with compounds from other groups and is the reason behind the *n*-type character. This is also the case for thiospinels, which also exhibit promising thermoelectric performances, in particular owing to a fairly low lattice contribution to the thermal conductivity (Fig. 9). While this feat is common to group E materials, the absence of cations in special positions (and thus with large ADP) leads to a slightly higher value than compounds such as $Cu_4Sn_7S_{16}$ or tetrahedrites. Consequently, significant reduction in lattice thermal conductivity can be achieved with doping in thiospinels while only moderate improvements are obtained for tetrahedrites and $Cu_4Sn_7S_{16}$ (Fig. 9).

Accepted Manuscript

10.1002/anie.202108686

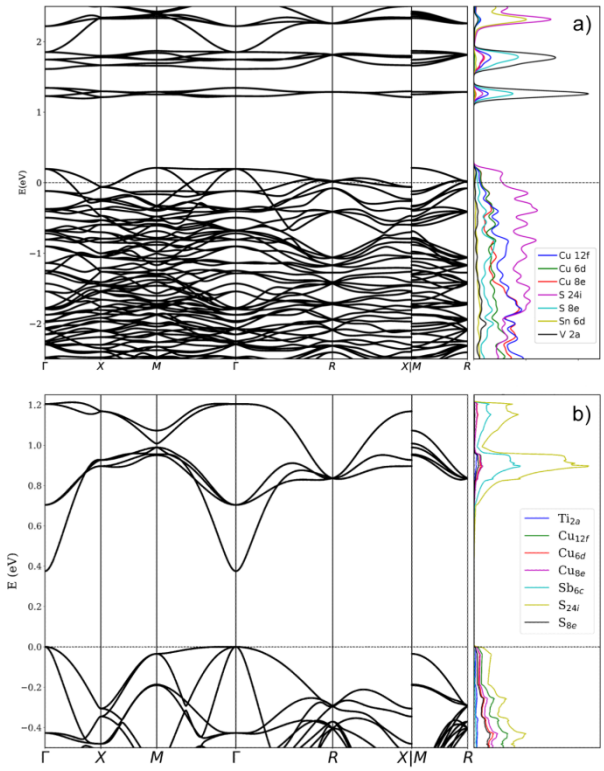

Figure 11 Electronic band dispersion and density of states for (a) $Cu_{26}V_2Sn_6S_{32}$ and (b) $Cu_{26}Ti_2Sb_6S_{32}$. Adapted with permission from Bourgès *et al.*,[78] copyright 2018 American Chemical Society, and Hagiwara *et al.*,[44] copyright 2021 American Chemical Society.

This final section focused on the structure-properties relationship in inorganic copper sulphides, we have emphasised the specific properties of materials in each group, in relation with the crystal structure and composition. The best thermoelectric performances are mainly achieved in *p*-type compounds with (i) disordered structures of group A/B and (ii) structures of group E containing atomic position with large ADP, owing to the intrinsically low thermal conductivity of cubic Cu_2SnS_3 derivatives, colusites and tetrahedrites (Fig. 9). To generate such high *ZT*, the materials must also exhibit high power factors. In performing ternary and quaternary *p*-type sulphides, regardless of the group, the materials have "relatively" similar band structures with the top of the valence band being mainly composed of Cu 3*d* and S 3*p* orbitals. The main difference between good and bad Cu-based thermoelectrics stands in the ability of the materials to adopt a Cu(I)-Cu(II) mixed valence, or in other words, to contain a certain number of holes per unit cell. This is mainly governed by the structure (cationic arrangement), composition and oxidation states of the elements. The best power factors are mainly obtained in "naturally" degenerate semiconductors, such as in colusites (group B), $Cu_5Sn_2S_7$ (group A), and tetrahedrites (group E), in which the Fermi level lies below the top of S-Cu manifold (Fig. 11a). Some "intrinsic" semiconductors, such as Cu_2SnS_3 (group A), famatinite Cu_3SbS_4 (group A) and colusite $Cu_{26}Ti_2Sb_6S_{32}$ (group B), Fig. 11b, if highly doped through cationic or anionic substitution, can also generate power factor values higher than 1.0 mW m^{-1} K^{-2} at high temperature. Of course, cationic ordering/disordering phenomena and microstructural features also affect the charge carrier mobility in the "Cu-S" network, and then the overall thermoelectric performances.

Accepted Manuscript

4. Conclusion

In this global analysis of the structure-properties relationship in inorganic copper sulphides associated with block *p* and *d* elements, we emphasised on the key role of the Cu(I) oxidation state and the importance of its tetrahedral coordination with respect to sulphur over its transport properties. In sulphides where Cu(I) is the majority cationic species, i.e. group A to D, the crystal structure is driven to adopt a framework where all cations are in tetrahedral coordination of sulphur. This leads to the formation of structures with a tetrahedral framework, derivative of either sphalerite or wurtzite crystal structures. These structures are remarkable by their tendency to form complex derivatives, either by cationic ordering within the *M*-S tetrahedral framework (group A), driven by electrostatic repulsion, or by adding "interstitial" *T* cations in the tetrahedral vacancies (group B to D). The additional TS_4 tetrahedra share edges and corners with the *M*-S tetrahedral framework, forming mixed $[TS_4]M_6$ tetrahedral-octahedral complexes, that can be either isolated from one-another (0D, group B), form 1D, 2D or 3D arrays of complexes (group C), or form a second network of corner-sharing TS_4 tetrahedra intertwined with the *M*-S tetrahedral framework (Group D). However, there are rare occasions where Cu does not impose the tetrahedral coordination to the rest of the cations. This is the case, for example, for CuS, $Cu_{12}Sb_4S_{13}$ or $Cu_4Sn_7S_{16}$ (Group E), in which Cu adopts different coordinations (triangular planar, octahedral, etc). This difference can be explained either by the occurrence of divalent copper, Cu(II), or the presence of a lone-pair of electrons or when Cu is a minority cationic species in the crystal structure.

Importantly, the concept of Cu(I)-Cu(II) mixed valence, corresponding to the presence of mobile charges on a Cu-S conductive network, is very much demonstrated and strongly dependant of both the Cu/*M* ratio and the crystal structure complexity of the material, two key parameters considered for the transport properties of these sulphides. It is worth pointing out that the structure classification, necessary for the understanding of chemical bond, can allow novel unconventional chemical bonds to be discovered, and consequently, can help to design materials with optimised properties. Moreover, the nature of the chemical bond is not the only parameter which governs the properties: structural distortions as well as cationic distributions in the structure (e.g. order-disorder phenomena) also influence significantly the electronic and thermal conductivity and consequently thermoelectricity. These parameters are of capital importance, together with doping effects to improve/optimise the properties of these materials. Thus the structure classification is a complementary approach to the strategy focused on designing chemical bonds for finding out novel functional inorganic copper sulphide materials.

Acknowledgements
The authors gratefully thank the financial support of the French Agence Nationale de la Recherche (ANR-15-CE05-0027) and FEDER and Normandy Region.

Keywords: Copper sulphides • Crystal structure• Thermoelectrics • Photovoltaics • Energy materials

Accepted Manuscript

References

[1] S. R. Rintoul, S. L. Chown, R. M. DeConto, M. H. England, H. A. Fricker, V. Masson-Delmotte, T. R. Naish, M. J. Siegert, J. C. Xavier, *Nature* **2018**, *558*, 233–241.
[2] D. M. Rowe, *Renew. Ener.* **1999**, *16*, 1251–1256.
[3] X.-L. L. Shi, J. Zou, Z.-G. G. Chen, *Chem. Rev.* **2020**, *120*, 7399–7515.
[4] Y.-X. Wang, W.-H. Lai, Y.-X. Wang, S.-L. Chou, X. Ai, H. Yang, Y. Cao, *Angew. Chemie Int. Ed.* **2019**, *58*, 18324–18337.
[5] A. V Powell, *J. Appl. Phys.* **2019**, *126*, 100901.
[6] R. Freer, A. V Powell, *J. Mater. Chem. C* **2020**, *8*, 441–463.
[7] G. Guélou, P. Lemoine, B. Raveau, E. Guilmeau, *J. Mater. Chem. C* **2021**, *9*, 773–795.
[8] K. Suekuni, T. Takabatake, *APL Mater.* **2016**, *4*, 104503.
[9] A. P. Gonçalves, E. B. Lopes, *Semiconductors* **2019**, *53*, 1817–1824.
[10] A. V Powell, in *Woodhead Publ. Ser. Electron. Opt. Mater.* (Ed.: R.B.T.-T.E.C. Funahashi), Woodhead Publishing, **2021**, pp. 183–196.
[11] K. Suekuni, M. Ohta, T. Takabatake, E. Guilmeau, in *Woodhead Publ. Ser. Electron. Opt. Mater.* (Ed.: R.B.T.-T.E.C. Funahashi), Woodhead Publishing, **2021**, pp. 197–216.
[12] S. Chen, A. Walsh, X.-G. Gong, S.-H. Wei, *Adv. Mater.* **2013**, *25*, 1522–1539.
[13] P. Kush, S. Deka, *ChemNanoMat* **2019**, *5*, 373–402.
[14] A. C. Lokhande, P. T. Babar, V. C. Karade, M. G. Gang, V. C. Lokhande, C. D. Lokhande, J. H. Kim, *J. Mater. Chem. A* **2019**, *7*, 17118–17182.
[15] A. Le Donne, V. Trifiletti, S. Binetti, *Front. Chem.* **2019**, *7*, 297.
[16] O. C. Olatunde, D. C. Onwudiwe, *Mater. Sci. Semicond. Process.* **2021**, *125*, 105627.
[17] A. C. Lokhande, R. B. V Chalapathy, M. He, E. Jo, M. Gang, S. A. Pawar, C. D. Lokhande, J. H. Kim, *Sol. Energy Mater. Sol. Cells* **2016**, *153*, 84–107.
[18] M. E. Fleet, *Zeitschrift für Krist. - Cryst. Mater.* **1970**, *132*, 276–287.
[19] Y. Goto, F. Naito, R. Sato, K. Yoshiyasu, T. Itoh, Y. Kamihara, M. Matoba, *Inorg. Chem.* **2013**, *52*, 9861–9866.
[20] P. Bonazzi, L. Bindi, G. P. Bernardini, S. Menchetti, *Can. Mineral.* **2003**, *41*, 639–647.
[21] S. R. Hall, J. M. Stewart, *Acta Crystallogr. Sect. B* **1973**, *29*, 579–585.
[22] M. Wintenberger, *Mater. Res. Bull.* **1979**, *14*, 1195–1202.
[23] S. C. Abrahams, J. L. Bernstein, *J. Chem. Phys.* **1973**, *59*, 5415–5422.
[24] J. Garin, E. Parthé, *Acta Crystallogr. Sect. B* **1972**, *28*, 3672–3674.
[25] L. M. de Chalbaud, G. D. de Delgado, J. M. Delgado, A. E. Mora, V. Sagredo, *Mater. Res. Bull.* **1997**, *32*, 1371–1376.
[26] M. Onoda, X. Chen, A. Sato, H. Wada, *Mater. Res. Bull.* **2000**, *35*, 1563–1570.
[27] V. Pavan Kumar, P. Lemoine, V. Carnevali, G. Guélou, O. I. Lebedev, P. Boullay, B. Raveau, R. Al Rahal Al Orabi, M. Fornari, C. Prestipino, et al., *J. Mater. Chem. A* **2021**, *9*, 10812.
[28] A. Pfitzner, S. Reiser, *Zeitschrift für Krist. - Cryst. Mater.* **2002**, *217*, 51.
[29] L. Pauling, S. Weinbaum, *Zeitschrift für Krist. - Cryst. Mater.* **1934**, *88*, 48.
[30] R. Shannon, *Acta Crystallogr. Sect. A* **1976**, *32*, 751–767.
[31] K. Chen, C. Di Paola, B. Du, R. Zhang, S. Laricchia, N. Bonini, C. Weber, I. Abrahams, H. Yan, M. Reece, *J. Mater. Chem. C* **2018**, *6*, 8546–8552.
[32] L. Pauling, R. Hultgren, *Zeitschrift für Krist.* **1933**, *84*, 204–212.
[33] J. T. Szymanski, *Can. Mineral.* **1976**, *14*, 529–535.

Accepted Manuscript

[34] H. Putz, W. H. Paar, D. Topa, E. Makovicky, A. C. Roberts, *Can. Mineral.* **2006**, *44*, 1481–1497.
[35] L. Bindi, H. Putz, W. H. Paar, C. J. Stanley, *Mineral. Mag.* **2017**, *81*, 1151–1159.
[36] Y. KUDOH, Y. TAKEUCHI, *Zeitschrift für Krist.* **1976**, *144*, 145–160.
[37] R. T. Tettenhorst, C. E. Corbato, *Am. Mineral.* **1984**, *69*, 943–947.
[38] S. R. Hall, E. J. Gabe, *Am. Mineral.* **1972**, *57*, 368–380.
[39] L. R. Bernstein, D. G. Reichel, S. Merlino, *Am. Mineral.* **1989**, *74*, 1177–1181.
[40] P. G. Spry, S. Merlino, Su Wang, Xiaomao Zhang, P. R. Buseck, *Am. Mineral.* **1994**, *79*, 750–762.
[41] L. Wenyuan, D. Cheng, G. Xiangping, L. Yu, Q. Xiaoping, C. Yuchuan, *Mineral. Mag.* **2014**, *78*, 1517–1525.
[42] Y. Kikuchi, Y. Bouyrie, M. Ohta, K. Suekuni, M. Aihara, T. Takabatake, *J. Mater. Chem. A* **2016**, *4*, 15207–15214.
[43] V. Pavan Kumar, A. R. Supka, P. Lemoine, O. I. Lebedev, B. Raveau, K. Suekuni, V. Nassif, R. Al Rahal Al Orabi, M. Fornari, E. Guilmeau, *Adv. Energy Mater.* **2019**, *9*, 1803249.
[44] T. Hagiwara, K. Suekuni, P. Lemoine, A. R. Supka, R. Chetty, E. Guilmeau, B. Raveau, M. Fornari, M. Ohta, R. Al Rahal Al Orabi, et al., *Chem. Mater.* **2021**, *33*, 3449–3456.
[45] V. Pavan Kumar, L. Paradis-Fortin, P. Lemoine, G. Le Caër, B. Malaman, P. Boullay, B. Raveau, G. Guélou, E. Guilmeau, *ACS Appl. Energy Mater.* **2019**, *2*, 7679–7689.
[46] M. Kars, A. Rebbah, H. Rebbah, *Acta Crystallogr. Sect. E* **2005**, *61*, i180--i181.
[47] G. E. Delgado, J. E. Contreras, A. J. Mora, S. Duran, M. Munoz, P. Grima-Gallardo, *Acta Phys. Pol. A* **2011**, *120*, 468–472.
[48] K. O. Klepp, D. Gurtner, *J. Alloys Compd.* **1996**, *243*, 19–22.
[49] E. A. Pruss, B. S. Snyder, A. M. Stacy, *Angew. Chemie Int. Ed. English* **1993**, *32*, 256–257.
[50] C. J. Crossland, J. S. O. Evans, *Chem. Commun.* **2003**, 2292–2293.
[51] S. R. Hall, J. F. Rowland, *Acta Crystallogr. Sect. B* **1973**, *29*, 2365–2372.
[52] J. F. Rowland, S. R. Hall, *Acta Crystallogaphica* **1975**, *B31*, 2105–2112.
[53] N. Morimoto, *Acta Crystallogr.* **1964**, *17*, 351–360.
[54] K. Yamamoto, S. Kashida, *J. Solid State Chem.* **1991**, *93*, 202–211.
[55] D. M. Trots, A. Senyshyn, D. A. Mikhailova, M. Knapp, C. Baehtz, M. Hoelzel, H. Fuess, *J. Phys. Condens. Matter* **2007**, *19*, 136204.
[56] Y. Kanazawa, K. Koto, N. Morimoto, *Can. Mineral.* **1978**, *16*, 397–404.
[57] K. Koto, N. Morimoto, *Acta Crystallogr. Sect. B* **1975**, *31*, 2268–2273.
[58] N. Le Nagard, G. Collin, O. Gorochov, *Mater. Res. Bull.* **1979**, *14*, 1411–1417.
[59] A. Choudhury, S. Mohapatra, H. Yaghoobnejad Asl, S. H. Lee, Y. S. Hor, J. E. Medvedeva, D. L. McClane, G. E. Hilmas, M. A. McGuire, A. F. May, et al., *J. Solid State Chem.* **2017**, *253*, 192–201.
[60] B. J. Wuensch, *Zeitschrift für Krist.* **1964**, *119*, 437–453.
[61] W. Lai, Y. Wang, D. T. Morelli, X. Lu, *Adv. Funct. Mater.* **2015**, *25*, 3648–3657.
[62] A. Suzumura, N. Nagasako, Y. Kinoshita, M. Watanabe, T. Kita, R. Asahi, *Mater. Trans.* **2015**, *56*, 858–863.
[63] S. O. Long, A. V Powell, S. Hull, F. Orlandi, C. C. Tang, A. R. Supka, M. Fornari, P. Vaqueiro, *Adv. Funct. Mater.* **2020**, *30*, 1909409.
[64] P. Vaqueiro, G. Guélou, A. Kaltzoglou, R. I. R. I. Smith, T. Barbier, E. Guilmeau, A. V. Powell, *Chem. Mater.* **2017**, *29*, 4080–4090.
[65] H. Xie, X. Su, X. Zhang, S. Hao, T. P. Bailey, C. C. Stoumpos, A. P. Douvalis, X. Hu, C. Wolverton, V. P. Dravid, et al., *J. Am. Chem. Soc.* **2019**, *141*, 10905–10914.

Accepted Manuscript

[66] P. Barahona, A. Galdámez, F. López-Vergara, V. Manríquez, O. Peña, *J. Solid State Chem.* **2014**, *212*, 114–120.
[67] X. Chen, H. Wada, A. Sato, M. Mieno, *J. Solid State Chem.* **1998**, *139*, 144–151.
[68] C. Bourgès, P. Lemoine, O. I. Lebedev, R. Daou, V. Hardy, B. Malaman, E. Guilmeau, *Acta Mater.* **2015**, *97*, 180–190.
[69] T. Barbier, P. Lemoine, S. Gascoin, O. I. Lebedev, A. Kaltzoglou, P. Vaqueiro, A. V. Powell, R. I. Smith, E. Guilmeau, *J. Alloys Compd.* **2015**, *634*, 253–262.
[70] G. Guélou, A. V. Powell, P. Vaqueiro, *J. Mater. Chem. C* **2015**, *3*, 10624–10629.
[71] K. Hashikuni, K. Suekuni, H. Usui, M. Ohta, K. Kuroki, T. Takabatake, *Appl. Phys. Lett.* **2016**, *109*, 182110.
[72] H. Xie, X. Su, G. Zheng, Y. Yan, W. Liu, H. Tang, M. G. Kanatzidis, C. Uher, X. Tang, *J. Phys. Chem. C* **2016**, *120*, 27895–27902.
[73] R. Zhang, K. Chen, B. Du, M. J. Reece, *J. Mater. Chem. A* **2017**, *5*, 5013–5019.
[74] V. Pavan Kumar, T. Barbier, V. Caignaert, B. Raveau, R. Daou, B. Malaman, G. Le Caër, P. Lemoine, E. Guilmeau, *J. Phys. Chem. C* **2017**, *121*, 16454–16461.
[75] Y. Yang, P. Ying, J. Wang, X. Liu, Z. Du, Y. Chao, J. Cui, *J. Mater. Chem. A* **2017**, *5*, 18808–18815.
[76] T. Barbier, D. Berthebaud, R. Frésard, O. I. Lebedev, E. Guilmeau, V. Eyert, A. Maignan, *Inorg. Chem. Front.* **2017**, *4*, 424–432.
[77] V. Pavan Kumar, L. Paradis-Fortin, P. Lemoine, V. Caignaert, B. Raveau, B. Malaman, G. Le Caër, S. Cordier, E. Guilmeau, *Inorg. Chem.* **2017**, *56*, 13376–13381.
[78] C. Bourgès, Y. Bouyrie, A. R. Supka, R. Al Rahal Al Orabi, P. Lemoine, O. I. Lebedev, M. Ohta, K. Suekuni, V. Nassif, V. Hardy, et al., *J. Am. Chem. Soc.* **2018**, *140*, 2186–2195.
[79] B. Du, R. Zhang, M. Liu, K. Chen, H. Zhang, M. J. Reece, *J. Mater. Chem. C* **2019**, *7*, 394–404.
[80] K. Suekuni, Y. Shimizu, E. Nishibori, H. Kasai, H. Saito, D. Yoshimoto, K. Hashikuni, Y. Bouyrie, R. Chetty, M. Ohta, et al., *J. Mater. Chem. A* **2019**, *7*, 228–235.
[81] Q. Jiang, H. Yan, Y. Lin, Y. Shen, J. Yang, M. J. Reece, *J. Mater. Chem. A* **2020**, *8*, 10909–10916.
[82] T. Deng, T. Xing, M. K. Brod, Y. Sheng, P. Qiu, I. Veremchuk, Q. Song, T.-R. Wei, J. Yang, G. J. Snyder, et al., *Energy Environ. Sci.* **2020**, *13*, 3041–3053.
[83] T. Tanimoto, K. Suekuni, T. Tanishita, H. Usui, T. Tadano, T. Kamei, H. Saito, H. Nishiate, C. H. Lee, K. Kuroki, et al., *Adv. Funct. Mater.* **2020**, *30*, 2000973.
[84] C. Bourgès, R. Al Rahal Al Orabi, Y. Miyazaki, *J. Alloys Compd.* **2020**, 154240.
[85] M. L. Liu, F. Q. Huang, L. D. Chen, I. W. Chen, *Appl. Phys. Lett.* **2009**, *94*, 202103.
[86] Y.-X. Chen, B.-P. Zhang, Z.-H. Ge, P.-P. Shang, *J. Solid State Chem.* **2012**, *186*, 109–115.
[87] X. Lu, D. T. Morelli, Y. Xia, F. Zhou, V. Ozolins, H. Chi, X. Zhou, C. Uher, *Adv. Energy Mater.* **2013**, *3*, 342–348.
[88] Y. Shen, C. Li, R. Huang, R. Tian, Y. Ye, L. Pan, K. Koumoto, R. Zhang, C. Wan, Y. Wang, *Sci. Rep.* **2016**, *6*, 32501.
[89] M. A. Green, E. D. Dunlop, J. Hohl-Ebinger, M. Yoshita, N. Kopidakis, A. W. Y. Ho-Baillie, *Prog. Photovoltaics Res. Appl.* **2020**, *28*, 3–15.
[90] H. Hiroi, Y. Iwata, S. Adachi, H. Sugimoto, A. Yamada, *IEEE J. Photovoltaics* **2016**, *6*, 760–763.
[91] L. Xi, Y. B. Zhang, X. Y. Shi, J. Yang, X. Shi, L. D. Chen, W. Zhang, J. Yang, D. J. Singh, *Phys. Rev. B* **2012**, *86*, 155201.
[92] B. Raveau, *J. Supercond. Nov. Magn.* **2019**, *33*, 259–263.

Accepted Manuscript

[93] H. Zhao, X. Xu, C. Li, R. Tian, R. Zhang, R. Huang, Y. Lyu, D. Li, X. Hu, L. Pan, et al., *J. Mater. Chem. A* **2017**, *5*, 23267–23275.
[94] L. Zhao, C. Chen, L. Pan, X. Hu, C. Lu, Y. Wang, *J. Appl. Phys.* **2019**, *125*, 95107.
[95] W. Zhou, P. Dwivedi, C. Shijimaya, M. Ito, K. Higashimine, T. Nakada, M. Takahashi, D. Mott, M. Miyata, M. Ohta, et al., *ACS Appl. Nano Mater.* **2018**, *1*, 4819–4827.
[96] W. Zhou, C. Shijimaya, M. Takahashi, M. Miyata, D. Mott, M. Koyano, M. Ohta, T. Akatsuka, H. Ono, S. Maenosono, *Appl. Phys. Lett.* **2017**, *111*, 263105.
[97] V. Pavan Kumar, P. Lemoine, V. Carnevali, G. Guélou, O. I. Lebedev, B. Raveau, R. Al Rahal Al Orabi, M. Fornari, C. Candolfi, C. Prestipino, et al., *Inorg. Chem.* **2021**, submitted.
[98] H. Xie, X. Su, S. Hao, C. Zhang, Z. Zhang, W. Liu, Y. Yan, C. Wolverton, X. Tang, M. G. Kanatzidis, *J. Am. Chem. Soc.* **2019**, *141*, 18900–18909.
[99] D. Zou, G. Nie, Y. Li, Y. Xu, J. Lin, H. Zheng, J. Li, *RSC Adv.* **2015**, *5*, 24908–24914.
[100] T. Tanishita, K. Suekuni, H. Nishiate, C.-H. Lee, M. Ohtaki, *Phys. Chem. Chem. Phys.* **2020**, *22*, 2081–2086.
[101] H. Hiroi, N. Sakai, T. Kato, H. Sugimoto, in *2013 IEEE 39th Photovolt. Spec. Conf.*, **2013**, pp. 863–866.
[102] A. McEvoy, L. Castaner, T. Markvart, *Solar Cells: Materials, Manufacture and Operation*, Academic Press, **2012**.
[103] V. Itthibenchapong, R. S. Kokenyesi, A. J. Ritenour, L. N. Zakharov, S. W. Boettcher, J. F. Wager, D. A. Keszler, *J. Mater. Chem. C* **2013**, *1*, 657–662.
[104] K. Suekuni, K. Tsuruta, M. Kunii, H. Nishiate, E. Nishibori, S. Maki, M. Ohta, A. Yamamoto, M. Koyano, *J. Appl. Phys.* **2013**, *113*, 043712.
[105] T. He, N. Lin, Z. Du, Y. Chao, J. Cui, *J. Mater. Chem. C* **2017**, *5*, 4206–4213.
[106] E. M. Chen, S. S. Stoyko, J. A. Aitken, P. F. P. Poudeu, *Inorg. Chem. Front.* **2017**, *4*, 1493–1500.
[107] X. Qiu, P. Qiu, T. Deng, H. Huang, X. Du, X. Shi, L. Chen, *Zeitschrift fur Anorg. und Allg. Chemie* **2020**, *646*, 1116–1121.
[108] Y. Goto, Y. Sakai, Y. Kamihara, M. Matoba, *J. Phys. Soc. Japan* **2015**, *84*, 44706.
[109] X. Lu, D. T. Morelli, Y. Xia, V. Ozolins, *Chem. Mater.* **2015**, *27*, 408–413.
[110] K. Suekuni, F. S. Kim, T. Takabatake, *J. Appl. Phys.* **2014**, *116*, 063706.
[111] K. Suekuni, F. S. Kim, H. Nishiate, M. Ohta, H. I. Tanaka, T. Takabatake, *Appl. Phys. Lett.* **2014**, *105*, 132107.
[112] I. Siloi, P. Gopal, S. Curtarolo, M. Buongiorno Nardelli, P. Vaqueiro, M. Fornari, *ACS Appl. Energy Mater.* **2019**, DOI 10.1021/acsaem.9b01564.
[113] G. Guélou, V. Pavan Kumar, A. Bourhim, P. Lemoine, B. Raveau, A. Supka, O. I. Lebedev, R. Al Rahal Al Orabi, M. Fornari, K. Suekuni, et al., *ACS Appl. Energy Mater.* **2020**, *3*, 4180–4185.
[114] G. Guélou, C. Couder, A. Bourhim, O. I. Lebedev, N. Daneu, F. Appert, J. Juraszek, P. Lemoine, L. Segreto, E. Guilmeau, *Acta Mater.* **2020**, *195*, 229–239.
[115] Y. Yu, M. Cagnoni, O. Cojocaru-Mirédin, M. Wuttig, *Adv. Funct. Mater.* **2020**, *30*, 1904862.
[116] M. Cagnoni, D. Führen, M. Wuttig, *Adv. Mater.* **2018**, *30*, 1801787.
[117] G. Tan, L. D. Zhao, M. G. Kanatzidis, *Chem. Rev.* **2016**, *116*, 12123–12149.
[118] D. Sarkar, S. Roychowdhury, R. Arora, T. Ghosh, A. Vasdev, B. Joseph, G. Sheet, U. V Waghmare, K. Biswas, *Angew. Chem. Int. Ed. Engl.* **2021**, *60*, 10350–10358.
[119] V. Pavan Kumar, G. Guélou, P. Lemoine, B. Raveau, A. Supka, R. Al Rahal Al Orabi, M. Fornari, K. Suekuni, E. Guilmeau, *Angew. Chemie Int. Ed.* **2019**, *58*, 15455–15463.
[120] L. Paradis-Fortin, G. Guélou, V. Pavan Kumar, P. Lemoine, C. Prestipino, O.

Accepted Manuscript

Merdrignac-Conanec, G. R. Durand, S. Cordier, O. I. Lebedev, E. Guilmeau, *J. Alloys Compd.* **2020**, *831*, 154767.
[121] A. B. Kehoe, D. O. Scanlon, G. W. Watson, *J. Mater. Chem. C* **2015**, *3*, 12236–12244.
[122] H. Arribart, B. Sapoval, O. Gorochov, N. LeNagard, *Solid State Commun.* **1978**, *26*, 435–439.
[123] A. Golub, N. Allali, D. Guyomard, M. Danot, *Mater. Res. Bull.* **1995**, *30*, 959–966.
[124] Z.-H. Ge, L.-D. Zhao, D. Wu, X. Liu, B.-P. Zhang, J.-F. Li, J. He, *Mater. Today* **2016**, *19*, 227–239.
[125] G. Dennler, R. Chmielowski, S. Jacob, F. Capet, P. Roussel, S. Zastrow, K. Nielsch, I. Opahle, G. K. H. H. Madsen, *Adv. Energy Mater.* **2014**, *4*, 1301581.
[126] P. Qiu, T. Zhang, Y. Qiu, X. Shi, L. Chen, *Energy Environ. Sci.* **2014**, *7*, 4000–4006.
[127] S. O. J. Long, A. V Powell, P. Vaqueiro, S. Hull, *Chem. Mater.* **2018**, *30*, 456–464.
[128] P. Lemoine, C. Bourgès, T. Barbier, V. Nassif, S. Cordier, E. Guilmeau, *J. Solid State Chem.* **2017**, *247*, 83–89.
[129] K. Suekuni, K. Tsuruta, T. Ariga, M. Koyano, *Appl. Phys. Express* **2012**, *5*, 2–5.
[130] K. Suekuni, C. H. Lee, H. I. Tanaka, E. Nishibori, A. Nakamura, H. Kasai, H. Mori, H. Usui, M. Ochi, T. Hasegawa, et al., *Adv. Mater.* **2018**, *30*, 1706230.
[131] J. Heo, R. Ravichandran, C. F. Reidy, J. Tate, J. F. Wager, D. A. Keszler, *Adv. Energy Mater.* **2015**, *5*, 1401506.
[132] M. Hasaka, T. Aki, T. Morimura, S.-I. Kondo, *Energy Convers. Manag.* **1997**, *38*, 855–859.
[133] M. T. Caldes, C. Guillot-Deudon, A. Thomere, M. Penicaud, E. Gautron, P. Boullay, M. Bujoli-Doeuff, N. Barreau, S. Jobic, A. Lafond, *Inorg. Chem.* **2020**, *59*, 4546–4553.
[134] T. Deng, T.-R. Wei, Q. Song, Q. Xu, D. Ren, P. Qiu, X. Shi, L. Chen, *RSC Adv.* **2019**, *9*, 7826–7832.
[135] J. P. F. Jemetio, P. Zhou, H. Kleinke, *J. Alloys Compd.* **2006**, *417*, 55–59.

Entry for the Table of Contents

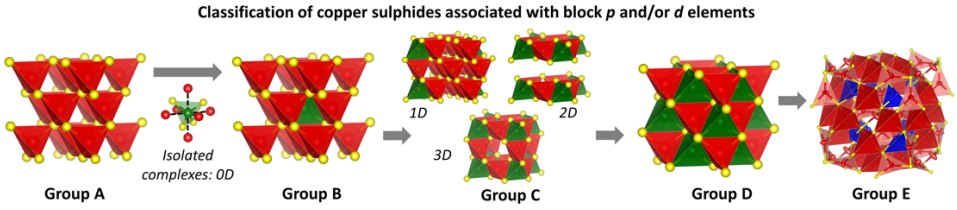

A classification of copper-sulphides based on crystallographic features is proposed. It arises from thorough investigations of the structure-properties relationships in these phases, over dozens of publications in the fields of crystallography and materials for energy conversion. This classification reveals systematic trends that can be explained and exploited for the design and engineering of new environmentally-friendly materials.

Accepted Manuscript